REMAINING LIFE ASSESSMENT OF STEAM TURBINE AND HOT GAS EXPANDER COMPONENTS

David Dowson
Service Engineer (Materials & Repairs)
Elliott Group
Jeannette, PA, USA

David Dowson is a Service Engineer with the Elliott Group, in Jeannette, Pennsylvania. He has been involved with material related failure analysis, repairs to rotating and non-rotating equipment, and aftermarket support. He has co-authored papers on materials selection for hot gas expanders, repairs to turbomachinery components, defect tolerant design concepts and remaining life assessment. Mr. Dowson received his B.S. degree (2003) from the University of Pittsburgh.

Derrick Bauer
Manager, Materials Engineering
Elliott Group
Jeannette, PA, USA

Derrick joined Elliott Group in 2002 as a Materials Engineer. He has been involved with R&D projects, production and aftermarket support, failure analysis and remaining life assessment testing. He received an MS from the University of Pittsburgh in 2011.

ABSTRACT

In today's market place, a large percentage of oil refinery, petrochemical, and power generation plants throughout the world have been trying to reduce their operation cost by extending the service life of their critical machines, such as steam turbines and hot gas expanders, beyond the design life criteria. The key ingredient in plant life extension is Remaining Life Assessment Technology. This paper will outline the Remaining Life Assessment procedures, and review the various damage mechanisms such as creep, fatigue, creep-fatigue and various embrittlement mechanisms that can occur in these machines. Also highlighted will be the various testing methods for determining remaining life or life extension of components such as high precision SRT (Stress Relaxation Test), which determines creep strength, and CDR (Constant Displacement Rate) Test, which evaluates fracture resistance. Other tests such as replication/microstructure analysis and toughness tests will be reviewed for assessment of the remaining life or life extension of the components. Use of computer software will be highlighted showing how creep-life, fatigue-life and creep/fatigue-life calculations can be performed. Actual examples of remaining life assessment testing performed on steam turbines and hot gas expander components are provided.

INTRODUCTION

In recent years, from oil refinery to petrochemical and power generation industries, more and more plants throughout the world are facing a common issue – aging turbines, usually over 30 years old. Questions bearing in managers' mind are what is the machine condition and whether they can be continually operated (if yes, how long). The answer is significant not only for safety concern but also for cost reduction, especially with today's limited budget. Therefore, there is an increasingly strong desire for the engineering aftermarket service to perform "Remaining Life Assessment" of steam turbines and hot gas expanders.

Remaining life assessment is to use metallurgical and fracture mechanics methodologies to predict the remaining life of structures and components that have been in service for an extended period of time, usually close to or beyond the designed life. Traditionally, if parts are found with material degradations or damages during an overhaul, they might be scrapped and replaced for risk-free consideration; even though they might have some useful life. Remaining life assessment offers a possible tool to estimate the useful remaining lifetime and avoid premature scrapping of the parts. Remaining life

assessment is considered to be an attractive method/process for cost reduction and for minimizing down-time.

Remaining life assessment has often been improperly referred as "life extension". Actually this analysis will not extend the lifetime of the components. It can only assess the useful remaining lifetime, based on the metallurgical examinations and theoretical (fracture mechanics) calculations. If such assessments indicate the need for extensive replacements and refurbishments, life extension may not prove to be a viable option. Above and beyond this objective, remaining life assessment technology serves many other purposes. It helps in setting up proper inspection schedules, maintenance procedures and operating procedures. It should, therefore, be recognized at the outset that development of techniques for remaining life assessment is more enduring in value and broader in purpose than simply the extension of plant life. For instance, it has been possible to extend the inspections from six to ten year for modern rotors, on the basis of assessments from fracture mechanics calculations, resulting in considerable savings.

In implementing remaining life assessment procedures, the appropriate failure definition applicable to a given situation must be determined at the outset, and the purpose for which the assessment is being carried out must be kept in mind. While determining the feasibility of extended plant life may be one objective, a more common objective is the setting of appropriate intervals for inspection, repair and maintenance. In this context, remaining life assessment procedures are used only to ascertain that failures will not occur between such intervals. It should never be assumed that having performed a remaining life assessment study for a 20-year life extension, one could then wait for 20 years without interim monitoring. Periodic checks to ensure the validity of the initial approach are essential. In this sense, remaining life assessment should be viewed as an on-going task, rather than a one-time activity.

A phased approach, in which the initial level includes non-incursive techniques followed by other levels of actual plant monitoring, then followed by nondestructive inspections and destructive tests would be the most logical and cost effective approach. In Level I, assessments are performed using plant records, design stresses and temperatures, and minimum values of material properties from the OEM. Level II involves actual measurements of dimensions, temperatures, simplified stress calculations and inspections coupled with the use of minimum material properties from the OEM. Level III involves in-depth inspection, stress levels, plant monitoring, and generation of actual material data from samples removed from the component (destructive testing). The degree of the detail and accuracy of the results increases from Level I to Level III, but at the same time, the cost of the assessment also increases. Depending on the extent of the information available and the results obtained, the analysis may stop at any level or proceed to the next level as necessary.

In evaluating the failure criteria or remaining life, one needs to understand the various failure mechanisms that can occur. In turbomachinery components, the failure criteria can be governed by one or a combination of the following failure mechanisms:

- Fatigue – high cycle or low cycle
- Corrosion / Corrosion Fatigue
- Stress Corrosion Cracking (SCC)
- Erosion – solid particle or liquid impingement
- Erosion Corrosion
- Embrittlement
- Creep Rupture / Creep Fatigue
- High Temperature Corrosion/Embrittlement
- Mechanical (foreign objective) Damage

However, in remaining life assessment, usually only those mechanisms depending on temperature & time are taken into account. For example, for turbine casing, engineers usually focus on thermal-stress induced low cycle fatigue, creep rupture, and tempering embrittlement cracking. These failures usually are slow processes, therefore, can be assessed and forecasted by examining the warning evidences in the material.

Countless works have been done to study the behaviors of fatigue crack initiation/propagation and creep or embrittlement rupture in materials. Scientists and engineers have reached to such a level that, by knowing the flaw size or microstructure deterioration/damage, one can theoretically calculate and predict the remaining lifetime of the parts, based on the knowledge of the material properties and understanding of the stress distributions.

FATIGUE

Failures that occur under cyclic loading are termed fatigue failures. These can be vibration stresses on blades, alternating bending loads on shafts, fluctuating thermal stresses during start-stop cycles, etc. There are two types of fatigue: low cycle fatigue (LCF), high cycle fatigue (HCF). Traditionally, low cycle fatigue failure is classified occurring below 10^4 cycles, and high cycle fatigue is above that number. An important distinction between HCF and LCF is that in HCF most of the fatigue life is spent in crack initiation, whereas in LCF most of the life is spent in crack propagation because cracks are found to initiate within three to 10 percent of the fatigue life. HCF is usually associated with lower stress, while LCF usually occurs under higher stress.

Remaining life of casings or rotating components is generally based upon crack growth consideration. Fracture mechanics is the mathematical tool that is employed. It provides the concepts and equations used to determine how cracks grow and their effect on the strength of the structure. At the author's company fracture mechanics is utilized in analyzing the structural integrity of components that have been in operation to determine whether the component is suitable for further operation. Based upon crack growth analysis one

considers a number of scenarios.

From an initial defect size a_o one must determine critical flaw size a_c for fast fracture.

$$a_o \rightarrow a_c$$
$$K_I \rightarrow K_{IC}$$

where:

K_I = applied tensile mode I stress intensity factor
K_{IC} = plane strain fracture toughness of material

For LCF, determine how many cycles for a_o to grow to a_c. For HCF, one must prevent crack growth. Consequently for HCF, $\Delta K_I < \Delta K_{th}$, where:

ΔK_I = stress intensity factor ksi $\sqrt{in}$.
ΔK_{th} = threshold stress intensity factor range below which fatigue crack growth (or corrosion fatigue crack growth) does not occur.

Further discussion of fracture mechanic concepts can be found elsewhere (Dowson, 1995, 1994).

CREEP RUPTURE AND STRESS RUPTURE

Evidence of creep damage in the high temperature regions of blade attachment areas of rotors has been observed in some instances (Bush, 1982). The rim stresses and metal temperature at these locations are assessed against the creep rupture data for that particular grade of steel/or material. Traditionally one has used a Larson Miller (LM) plot of the type shown in Figure 1.
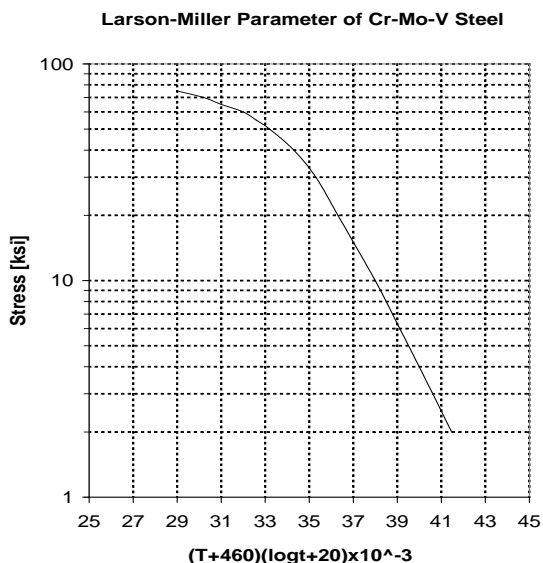
Larson-Miller Parameter of Cr-Mo-V Steel

Figure 1. Larson-Miller Curve of Cr-Mo-V alloy steel (ASTM A470 Class 8)

The degree of safety margin depends on the user and what lower bound design curve is applied. Since these curves are based upon the chemistry, variation in chemistry for a

particular grade can have an effect on the Larson Miller curve. Also, Larson Miller curves are generally based upon creep rupture tests done for 10^4 to 3×10^4 hours and very few data at 10^5 hours. Consequently, the data for longer hours is generally extrapolated. Since most of the creep rupture data is done with smooth bar specimens, the effect of notch ductility at long-term service has not been done. Short term notched bars tests may fail to predict the onset of notch sensitivity. Notch sensitively is not an inherent property but depends on the temperature, stress, stress state, and strain rate.

In assessing remaining life of components due to creep, such as blade attachments, crack initiation is used as the criteria. However, with the emergence of cleaner steel and fracture mechanics and an increasing need to extend life of component, application of crack growth, techniques have become common in the past decade.

For crack initiation as the fracture criteria, history-based calculation methods are often used to estimate life.

Methods For Crack Initiation Due To Creep

For the analytical method, one must have accurate operating history of the components which may consist of temperature, applied loads, changes in operation, such as shut downs or variation in speed or pressure. A simplistic estimation of the creep life expended can be made by assessing the relaxed long-term bore stresses and rim-stresses against the standard rupture data using the life fraction rule. The life fraction rule (LFR) states that at failure:

$$\sum \frac{t_i}{t_{ri}} = 1 \quad (1)$$

where:
t_i is the time spent at a given stress and temperature and t_{ri} is the rupture life for the same test conditions.

Example:

The purpose of this example is to illustrate the use of the life-fraction rule. A steam turbine piping system, made of 1-1/4 Cr-1/2Mo steel designed for a hoop stress of 7 ksi, was operated at 1000°F (538°C) for 42,500 h and at 1025°F (552°C) for the next 42,500 h. Calculate the life fraction expended using the life-fraction rule. From the Larson Miller Parameter curve of the steel, it is found that, at σ = 7 ksi,

t_{ri} at 1000°F = 220,000 h
t_{ri} at 1025°F = 82,380 h

Life fraction expended, t_i/t_{ri}, at 1000°F
$= \dfrac{42,500}{220,000} = 0.19$

Life fraction expended, t_i/t_{ri}, at 1025°F
$= \dfrac{42,500}{82,380} = 0.516$

The total life fraction expended is 0.71.

This rule was found to work well for small changes in stress and temperature especially for CrMoV rotor steel. However, for stress variations, the actual rupture lives were lower than the predicted values. Consequently, the LFR is generally valid for variable-temperature conditions as long as changing creep mechanisms and environmental interaction do not interfere with test results. However, the possible effect of material ductility on the applicability of the LFR needs to be investigated.

Non-Destructive Techniques

Conventional non-destructive evaluation (NDE) techniques fail to detect incipient damage which can be a precursor to crack initiation and subsequent rapid failure. However, there are other NDE techniques that have been developed for estimating the life consumption. These include microstructural techniques and hardness based techniques.

Metallographic Examination

Metallographic techniques have been developed that can correlate changes in the microstructure and the onset of incipient creep damage, such as triple point cavitation at the grain boundaries. For this technique, measurements by replication technique are taken on crack sensitive areas that are subjected to the higher temperatures and stresses. These areas are generally indicated by experience and analysis of previous damages.

The creep damage measured by replication is classified into four damage stages:
- Isolated cavities (A)
- Oriented cavities (B)
- Macrocracks (linking of cavities) (C)
- Formation of macrocracks (D)

The figure 2 shows the location of the four stages on the creep strain/exposure time curve (Neubauer and Wadel, 1983).
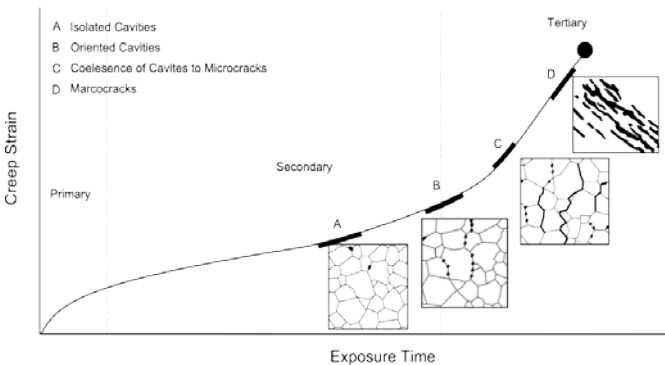

Figure 2. Replicas for Remaining Life Assessment.

In applying this approach Neubauer, et al., classified the stages into five stages which are Undamaged, Stage A, Stage B, Stage

C, and Stage D. These stages were corresponded roughly to expended life fractures (t/t_r) values of 0.27, 0.46, 0.65, 0.84 and 1 respectively using the conservative lower bound curve. Consequently, the remaining life can be calculated using the relationship as shown in Equation (2):

$$t_{rem} = t\left(\frac{t_r}{t} - 1\right) \qquad (2)$$

where: t is the service life expended and t_r is the rupture life.

For undamaged material and damaged stages A, B and C, the remaining life was found to be approximately 2.7t, 1.17t, 0.54t and 0.19t, respectively. Then by applying a safety factor of 3 to the calculations, the safe re-inspection intervals will become 0.9t, 0.4t, 0.18t and 0.06t respectively. This approach has been developed and implemented in the power generation industry (Viswanathan and Gehl, 1991). It was found to give increased inspection intervals as compared to the Neubauer and Wadel (1983) approach, as shown in Table 1.

Table 1. Suggested Reinspection Intervals for a plant with 30 years of Service.

Damage Classification	Inspection Interval (Years)	
	Wedel-Neubauer	EPRI-APTECH
Undamaged	5	27
A. Isolated Cavities	3	12
B. Oriented Cavities	1.5	5.4
C. Linked Cavities (Microcracks)	0.5	1.8
D. Macrocracks	Repair Immediately	Based on fracture mechanics

This approach has been applied by several utilities and realized significant savings in inspection costs. Other investigations indicate that there are wide variations in behavior due to differences in grain size, ductility and impurity control (Carlton, et al. 1967). For conservatism, the author's company adapted the Neubauer, et al., approach and classified the five stages as follows:

1) Undamaged material: Equipment can run and be re-inspected at next shutdown.
2) Class A – Re-inspection would be 3 to 5 years.
3) Class B – Re-inspection would be 1-1/2 to 3 years.
4) Class C – Replacement or repair would be needed within 6 months.
5) Class D – Immediate repair would be required.

Hardness Measurement

The first attempt to develop hardness as a technique to determine creep damage was by Goldhoff and Woodford (1972). In their study a good correlation was observed between

room temperature hardness measured on exposed creep specimens and the post exposure rupture life, Figure 3.
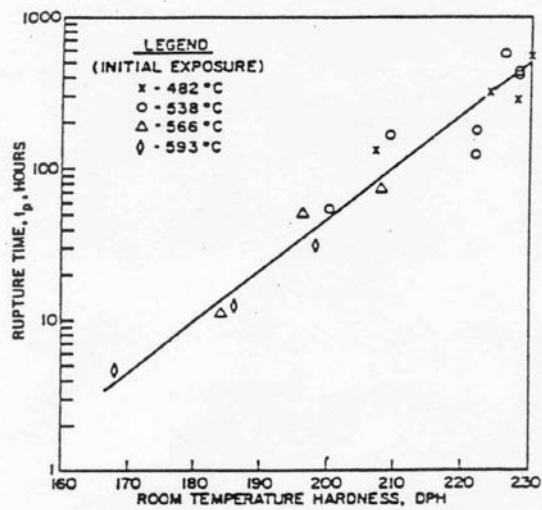

Figure 3. Correlation between post-exposure rupture time in the standard test at 538°C and 240 MPa and room temperature hardness for Cr-Mo-V rotor steel.

If similar calibration could be established between prior creep life expended or the remaining life fraction in the post exposure test and the hardness values for a range of CrMoV steels, this method could be applied to estimation of remaining life. However, data of this nature are not available in sufficient quantity. Other work done by Viswanathan and Gehl (1992) showed a lot of promise where he attempted to use the hardness technique as a stress indication. He observed that the application of stress accelerated the softening process and shifted the hardness to lower parameter values compared with the case of simple thermal softening on a plot of hardness vs. a modified Larson-Miller Parameter (Figure 4).
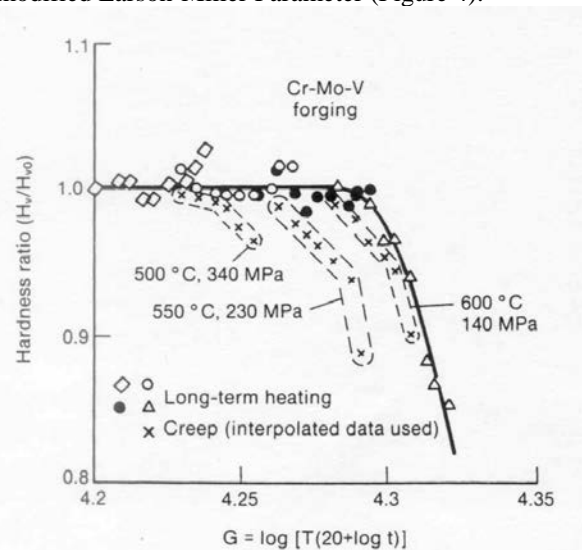
Figure 4. Plot of hardness ratio vs. G parameter for long-term heating and creep of Cr-Mo-V rotor steel.

Destructive Techniques

Newer tests to ascertain the useful life of used and/or repaired components have been utilized by the author's company. Design-For-Performance is a recently developed methodology for evaluating the creep strength and fracture resistance of high temperature materials. Whereas the traditional approach to creep design involves long-term testing and attempts to incorporate microstructural evolution in the test measurements, the new approach aims to exclude these changes in a short time high-precision test. The test may also be used to evaluate consequences of such changes in service-exposed samples. The new methodology recognizes that separate tests are necessary to measure creep strength and fracture resistance. For creep strength, a stress vs. creep rate response is determined from a stress relaxation test (SRT) and for fracture resistance a constant displacement rate (CDR) test of a notched temple specimen is performed at a temperature where the part is most vulnerable to fracture (Woodford, 1993).

Constant Displacement Rate Test

A description of the standardized CDR test is found elsewhere (Pope and Genyen, 1989). The data from the CDR test is tabulated in a curve similar to the load displacement curve for an ordinary elevated tensile test. For a typical tensile test fracture becomes unstable after the peak load is reached. On the other hand, in the CDR test, since the deformation is controlled at a constant rate and the notch is midway between the controlling extensometer, fracture rarely becomes unstable.

For a valid CDR test, the criteria for failure was considered to be the value of "displacement at fracture" was defined as the point of intersection of the 100 pound load line and the descending load displacement curve. The "displacement at failure" is measured from the start of the test to the point where the load displacement curve decreases below 100 pounds (Figure 5).
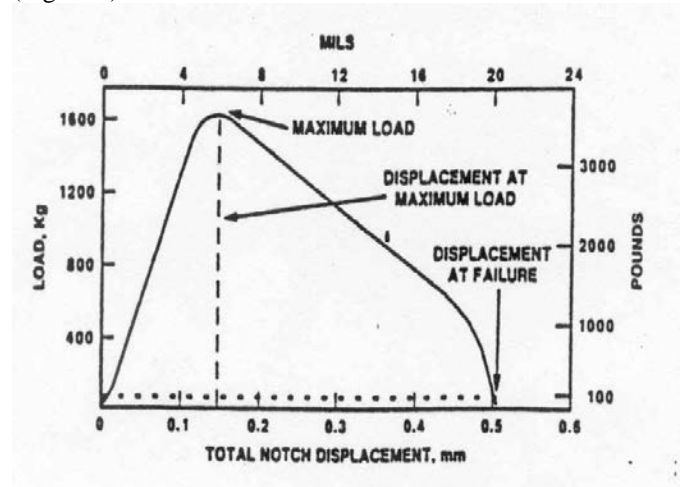

Figure 5. Example of Load Displacement Curve from CDR Tests at 1200°F and 2 mils/in/hr.

An example of how the environment can affect the notch sensitivity of the material is indicated by Figure 6. This example illustrates the effect of air exposure on IN738.
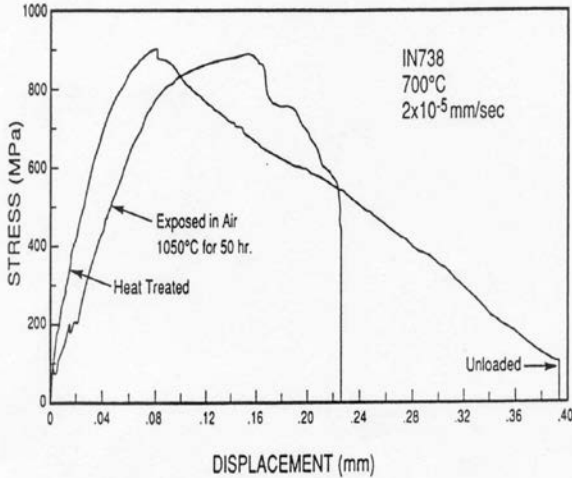

Figure 6. Constant Displacement Rate Tests Comparing Crack Growth Resistance in Heat Treated and Oxygen Embrittled Specimens.

Stress Relaxation Test

Specially designed samples for stress relaxation testing were tested on an Instron electromechanical series 8562 test system fitted with self-aligning grips, a 1500°C short furnace, and a capacitive extensometer. Details of the specimen geometry and extensometer sensitivity are provided elsewhere (Woodford, et al. 1992).

The standard test procedure involved loading the specimen at a fast rate of 10 MPa/sec (1,450 psi/sec) to a prescribed stress and then switching to strain control on the specimen and monitoring the relaxation stress. The inelastic (principally creep) strain-rate is calculated from the following equations, Equations (3) and (4).

$$\varepsilon_e + \varepsilon_I = \varepsilon_t = \text{Constant} \tag{3}$$

$$\dot{\varepsilon}_I = -\dot{\varepsilon}_e = -\frac{1}{E}\frac{d\sigma}{dt} \tag{4}$$

where:

ε_e is the elastic strain, $\dot{\varepsilon}_e$ is the elastic strain rate, ε_I is the inelastic strain (principally creep strain), $\dot{\varepsilon}_I$ is the inelastic strain rate, ε_t is the total strain, σ is the stress, and E is the elastic modulus measured during loading. Using this procedure, stress vs. strain-rate curves were generated covering up to five orders of magnitude in strain-rate in a test lasting less than five hours.

An example of the data generated in such tests is provided in Figure 7 for Waspaloy material. This shows stress vs. predicted time to one percent creep for Waspaloy. By utilizing this data one can plot a stress vs. Larson-Miller parameter for one percent predicted creep of Waspaloy compared to rupture data (Figure 8). From the data shown on the curve, the stress relaxation test can generate creep-stress rupture data in less than a few weeks as compared to traditional approach which incorporates long time testing.
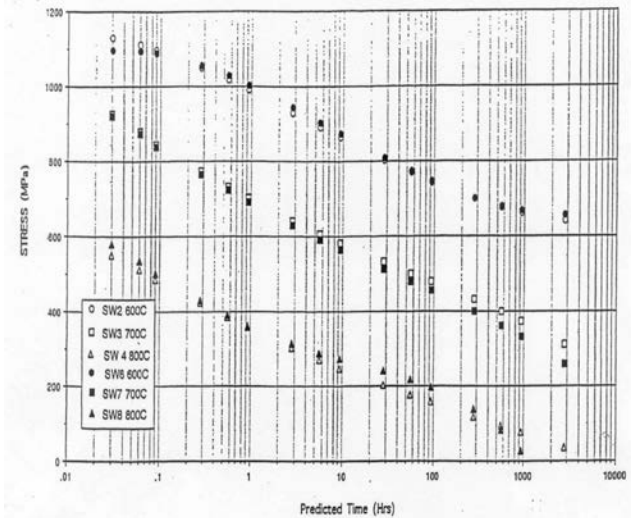

Figure 7. Stress vs. Predicted Times to 1% Creep for Standard Waspaloy.
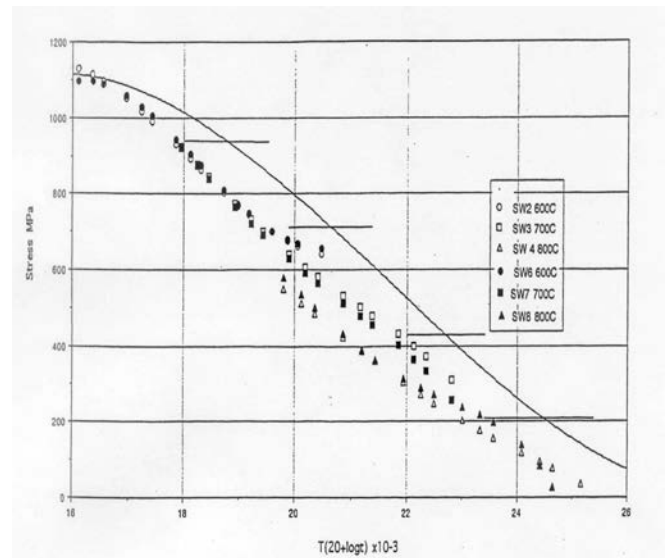

Figure 8. Stress vs. Larson-Miller Parameter for 1% Predicted Creep of Standard Waspaloy Compared with Rupture Data.

One major objective to this framework has been that effects of very long time exposures which could influence stress rupture life will not be accounted for. However, Woodford believes that such effect i.e. precipitation of

embrittling phases and grain boundary segregation of harmful elements are expected to influence the fracture resistance rather than creep resistance. The author's company has utilized this methodology to generate data for high temperature materials and weldments. Current methods are being developed for miniature specimens taken from serviced blades. From this data, it is envisioned that establishment of a set of minimum performance criteria which will enable repair/rejuvenation/replacement decision to be made.

CREEP/FATIGUE INTERACTION

For components that operate at higher temperature where creep growth can occur, one must take into account of the creep crack growth at intervals during the fatigue life of the component. The following is an example of a high temperature steam turbine rotor that failed catastrophically at Gallatin Power Plant in Tennessee (Saxena, 1998). The author will utilize computer software to demonstrate how creep-life, fatigue life and creep/fatigue-life calculations can be performed, and how inaccurate the calculation would be without accounting the creep life.

The Gallatin rotor was operated for 106,000 hours and had incurred 105 cold starts and 183 hot starts. The material was 1 CR- 1 Mo – 0.25V forging and had operated at a temperature of 800°F. The cracks originated from several MnS clusters with the original flaw size of 0.254" x 5.51" and 0.7" from the bore of the rotor (Figure 9).
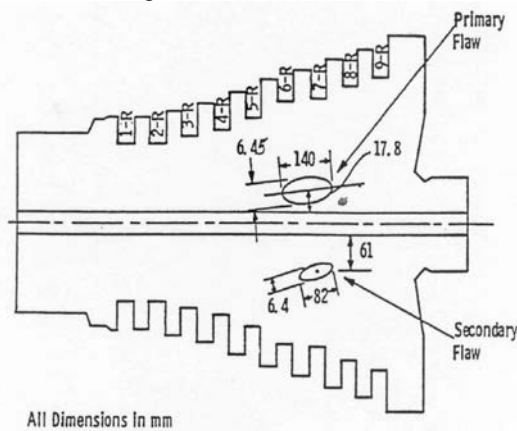

Figure 9. Schematic of the intermediate pressure (IP) section of the rotor showing the size and location of the primary and secondary flaws beneath the seventh row (7-R) of blades.
.

Step 1. Assessment of low cycle fatigue life.
The principle is that fatigue crack growth follows equation such as Paris Law:

$$\frac{da}{dN} = C_f \Delta K^n_f \qquad (5)$$

C_f and n_f are constants that depend on the material and environment.

The stress intensity factor range ΔK depends on the stress level at the crack tip. The life assessment criteria is that critical crack size a_c is not to be exceeded. In other words,

$$a \leq a_c$$

Figure 10 and Figure 11 show the stress intensity factor calculation together with the crack model that was used.
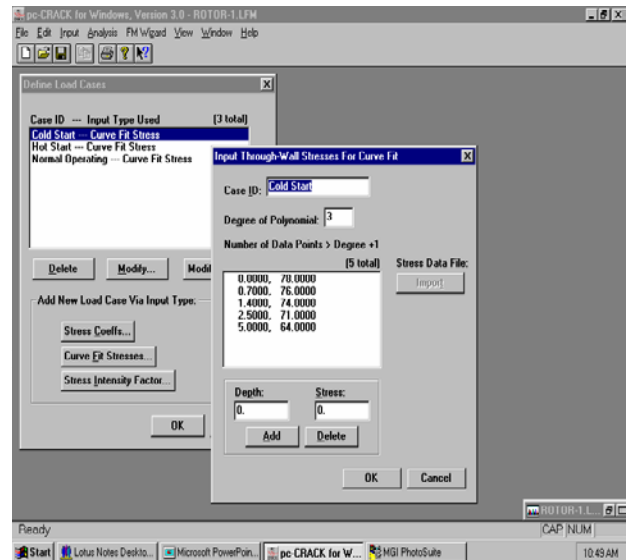

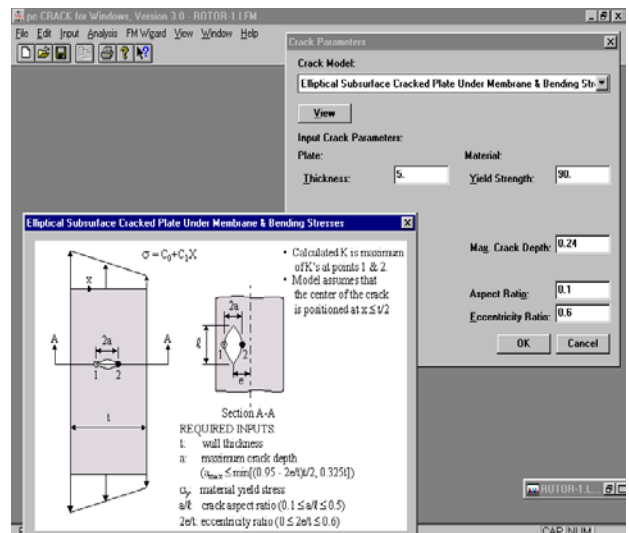*Figure 10. Computer Software Module. Stress Intensity Factor Calculation.*

Figure 11. Computer Software Module - Elliptical Subsurface Cracked Plate under Membrane and Bending Stresses.

By computing the information a plot of stress intensity factor

verses crack depth was done. Based on the plane strain fracture toughness of the material, the critical crack size 0.42" for cold start and 0.48" for hot start were determined, Figure 12.
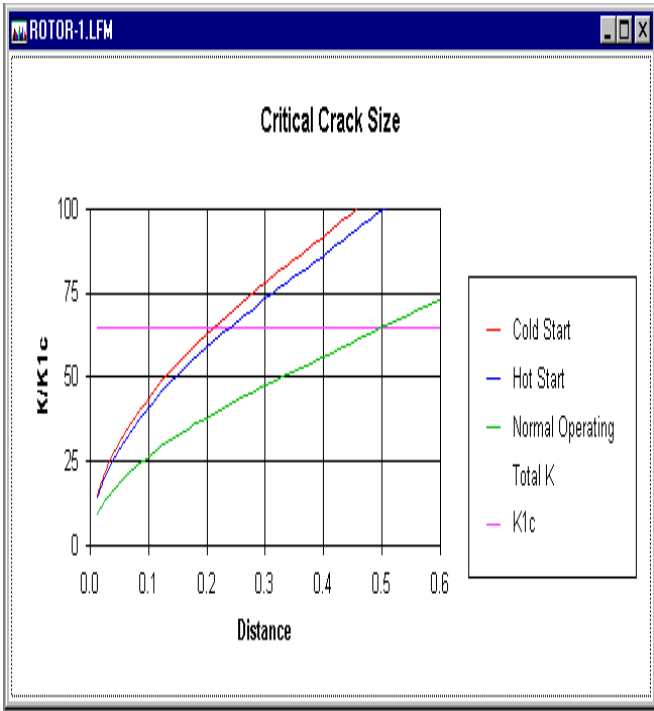

Figure 12. Critical Crack Size Calculation: The Critical Crack Size a_c is 0.42" for Cold Start and 0.48" for Hot Start.

Fatigue crack growth using Paris Law was computerized, Figure 13, Figure 14, and the low cycle fatigue crack growth was determines for both cold and hot starts.
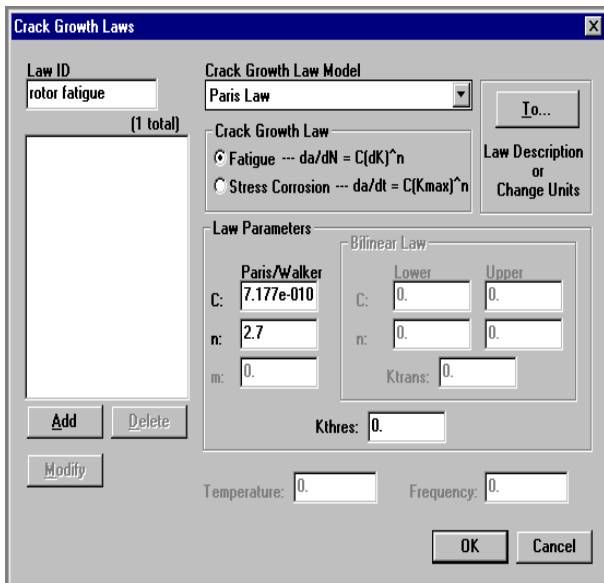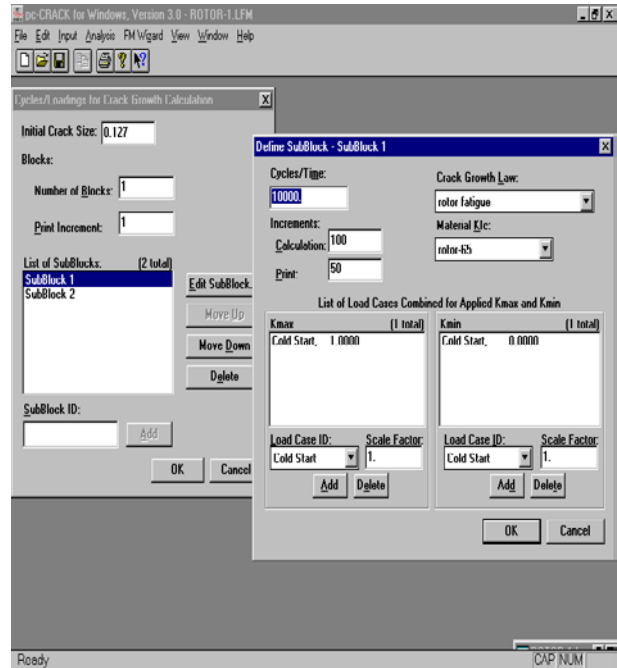

Figure 13. Fatigue Crack Growth.

Figure 14. Fatigue Crack Growth Calculation Model.

Figure 15 shows the low cycle fatigue crack growth which does not compare very well with that of the real life.
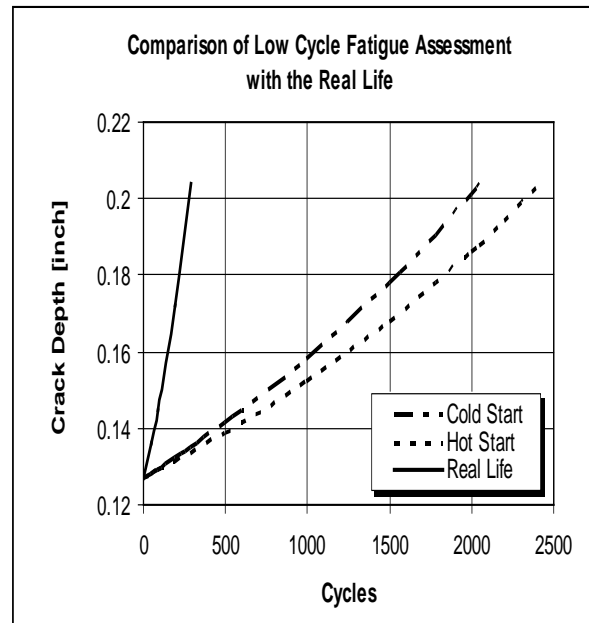

Figure 15. Shows Low Cycle Fatigue Crack Growth for Cold and Hot Starts Compared to Real Life.

The reason for the calculated life being much longer than the real life is that the hold time effect (or creep cracking effect) is not taken into account. Consequently, one must run a creep-fatigue remaining life assessment. The principle is that high temperature crack propagation is the summation of high

temperature fatigue plus primary creep plus secondary creep.

Creep-Fatigue Crack Growth: (6)

$$\frac{da}{dt} = \underbrace{C_c[C_t(t)]^q}_{\text{Creep}} + \underbrace{\frac{C_f}{h}(\Delta K)^{n_f}}_{\text{Fatigue}}$$

where:

h is the hold time in each cycle (which is 368 hours in this case).

The creep crack driving force is consisted of two parts:

(7)

$$C_t(t) = \underbrace{[C^*]^{2/[(1+p)(m-1)]}[\frac{(1-v^2)K^2}{E(n+1)t}]^{1-2/[(1+p)(m-1)]} + \frac{n+p+1}{(n+1)(p+1)}C_h^*(\frac{1}{t})^{p/(p+1)}}_{\text{Primary Creep}} + \underbrace{C^*}_{\text{Secondary Creep}}$$

The data that is inputted into the code is shown in Figure 16 and Figure 17. The calculation shows that, with accounting the creep effect, the creep-fatigue crack growth is much closer to the real life, Figure 18.
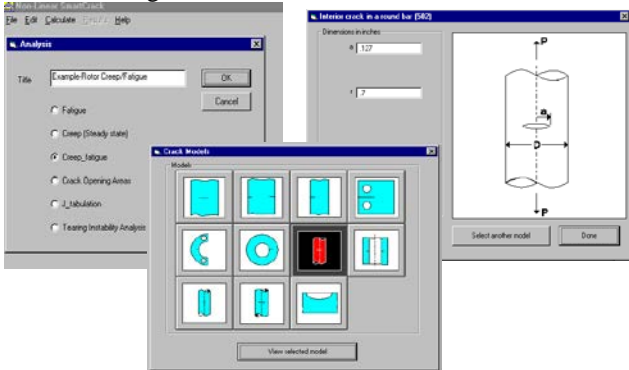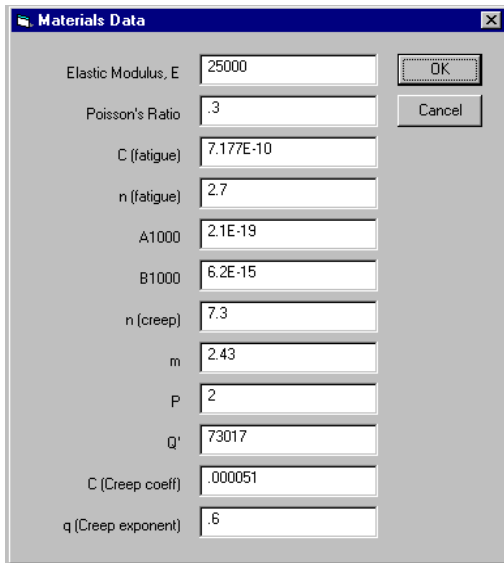

Figure 16. Creep/Fatigue Model.
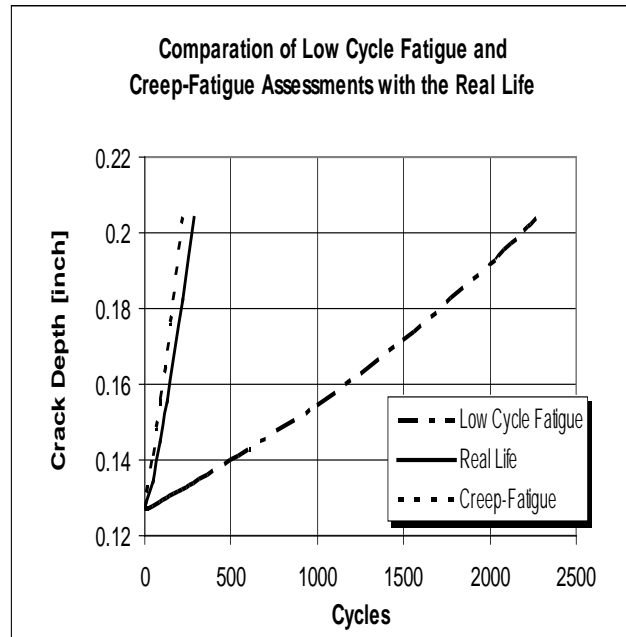

Figure 17. Creep/Fatigue Material Data.

Figure 18. Compares Low Cycle Fatigue and Creep-Fatigue Crack Growth to the Real Crack Growth.

This example demonstrates that if the material/component is operating in the creep mode, one must perform a creep-fatigue analysis instead of fatigue only. Generally a rule of thumb is that if only low cycle fatigue crack growth is counted and creep is not, then the calculated lifetime is about 10 times longer than the real life. By utilizing this software program, more accurate remaining life assessment can be achieved for materials operating in the creep regime under cyclic loading. Also, the lesson being learnt is that this rotor should have been examined by ultrasonic inspection every five years.

EMBRITTLEMENT

Trends toward increasing size and operating stresses in components, such as large turbine-generator rotors, require higher hardenability steels with increased strength and fracture toughness. However, higher hardenability steels especially those containing nickel and chromium are usually much more susceptible to a phenomena called temper embrittlement. The term temper embrittlement refers to a shift in the brittle-to-ductile transition temperature when steels/rotor shafts are heated or cooled slowly through the temperature range 660°F to 1060°F. This shift in the brittle-to-ductile transition temperature can be reversed by heating at a temperature of 1100°F or higher then fast cooled. Consequently, when examining rotor or casings that have been in service and operated within this temper embrittlement temperature range, the property toughness becomes an important criteria.

Evaluation of Toughness

Due to the advancement of fracture mechanics, it is now become possible to characterize toughness in terms of critical flaw size a_c. The definition of a_c depends on the conditions under which final rapid fracture occurs following the initial phase of sub-critical crack growth. At rotor grooves and rotor bores where final fracture is likely to occur at low temperatures during start-stop transients, a_c is dictated by linear elastic fracture mechanics. a_c is given by an expression of the form

$$K_{IC} = M\sigma\sqrt{\pi a_c} \quad (8)$$

where:
K_{IC} is the fracture toughness of the material or critical stress intensity for fracture, M is a constant to a given flaw size and geometry and σ is the nominal applied stress.
A typical loading sequence for turbine rotors shows variation in temperature and stress and their effect on critical flaw size a_c for cold start sequence (Viswanathan and Jaffee, 1983). Figure 19 shows the cold start sequence and associated variations in stress (σ), temperature (T) and critical flaw size (a_c) as function of time for the Gallatin rotor which failed catastrophically.
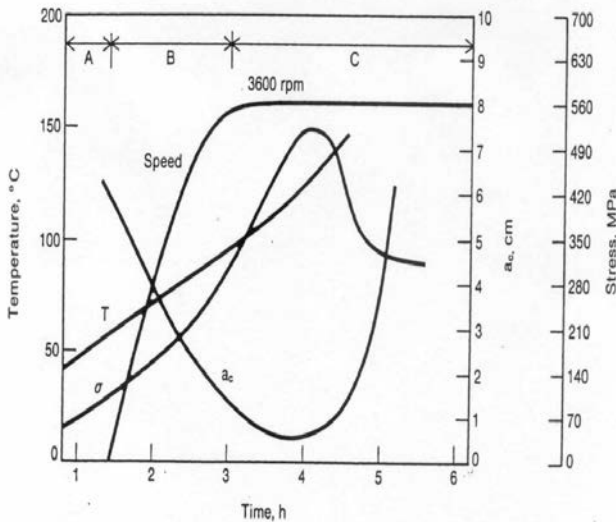

Figure 19. Illustration of cold-start sequence and associated variations in stress (σ), temperature (T), and critical flaw size (a_c) as functions of time from start.

The Region A consists of a warm up period after which the rotor was gradually brought up to speed (Region B). Once continuous operating speed was reached (Region C) approximately three hours after the warm up period, maximum loading was applied. Analysis of the failure location (7th row) showed that stresses reached a peak value of 74 ksi (520 MPa), 1-1/2 hours after the maximum continuous speed had been attained. The critical crack size reached its lowest value of 0.27" (6.9 mm) at temperature of 270°F (132°C) and 74 ksi (510 MPa). Since variation in temperature, stress, and material fracture toughness at the defect location can dictate the a_c value

for the rotor, one must calculate for the worst combination of these variables to prevent failure.

This can be done by using lower scatter band values of K_{IC}. However, to determine K_{IC} for rotors, large specimens need to be taken to satisfy the plane strain conditions required for a valid test. A more common practice is to determine the ductile-brittle fracture at transition temperature, FATT, using samples extracted from the periphery of a rotor and converting the FATT into K_{IC} using a correlation such as the one shown in Figure 20 (Schwant and Timo, 1985).
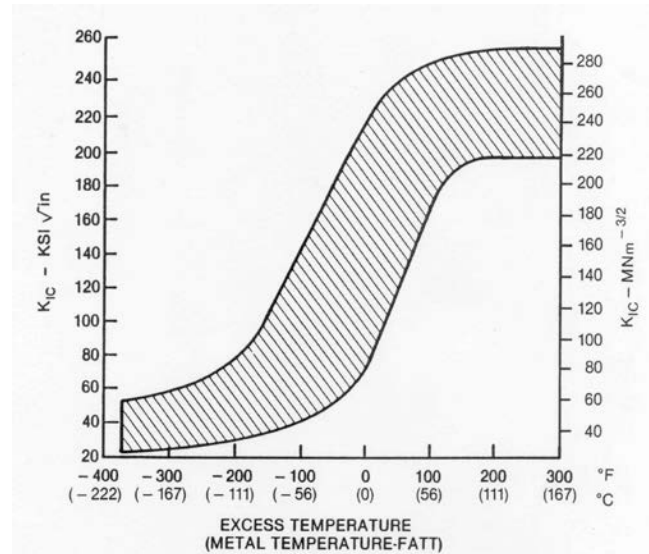

Figure 20. Turbine Rotor and Wheel Toughness Data.

Viswanathan and Gehl (1991) evaluated a number of data from numerous exposed CrMoV rotors and defined a lower threshold band for low alloy steels. The lower limit line for CrMoV steel is defined by the equation (Viswanathan and Wells, 1995) below:

$$K_{IC} = 95.042 + 0.5872\,T_E + 0.00168\,T_E^2 + 0.00000163 \quad (9)$$

where: K_{IC} is expressed in ksi $\sqrt{in}$ and T_E is the excess temperature (T – FATT) expressed in °F. Once the FATT is known, a K_{IC} verses temperature T curve can be established and used to determine a_c versus T.

However, such procedures tended to be conservative and there have been various other nondestructive and relatively destructive tests involving removal of very small samples to determine toughness of rotors. These techniques investigated include eddy-current examination, analytical electron microscope, secondary ion mass spectroscopy (SIMS), compositional correlations, Auger electron spectroscopy, chemical etching, use of single Charpy specimen and small punch tests. The techniques that show the most promise and have currently been applied in service application are:

- Correlation Based on Composition
- Small Punch Testing
- Chemical Etching

Correlation Based on Composition

An ASTM special task force on Large Turbine Generator Rotors of Subcommittee VI of ASTM Committee A-1 on steel has conducted a systematic study of the isothermal embrittlement at 750°F of vacuum carbon deoxidized (VCD) NiCrMoV rotor steels. Elements, such as P, Sn, As, Sb and Mo were varied in a controlled fashion and the shifts in FATT, (Δ) FATT were measured after 10,000 hours of exposure. From the results, the following correlations were observed in Equation (10):

$$\Delta \text{FATT} = 13544P + 12950\,\text{Sn} + 2100\,\text{As} - 93\,\text{Mo} - 810{,}000\,(P \times Sn) \quad (10$$

where: ΔFATT is expressed in °F and the correlation of all the elements are expressed in weight percent. According to this correlation, the elements P, Sn, and As increase temper embrittlement of steels, while Mo, P and Sn interaction decrease the temper embrittlement susceptibility.

All available 10,000 hour embrittlement data are plotted in Figure 21 as a function of calculated ΔFATT using Equation (10), (Newhouse, et al. 1972). A good correlation is observed between calculated and experimental ΔFATT. The scatter for this data is approximately ± 30°F for 750°F exposure and ±15°F for the 650°F exposure.
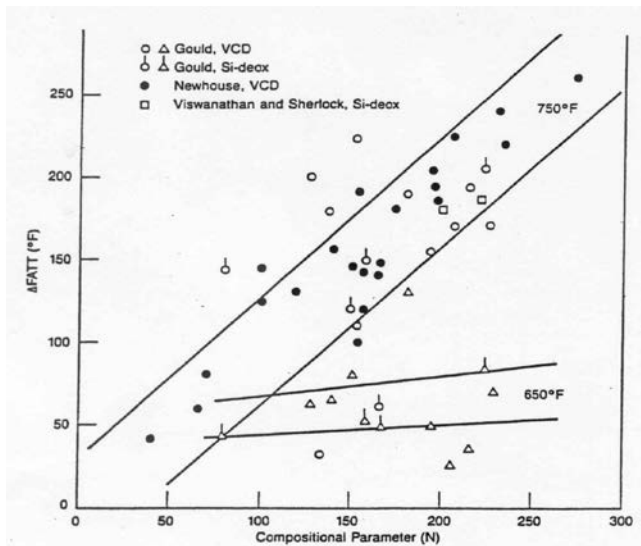

Figure 21. Correlation between compositional parameter "N" and the shift in FATT of NiCrMoV steels following exposure at 650°F and 750°F for 8800 hours.

Other correlations for determining the temper embrittlement susceptibility of steel, such as the J Factor proposed by Watanabe and Murakami (1981) and $\overline{X}$ Factor proposed by Bruscato (1970), are widely used.
These factors are given by:

$$J = (Si + Mn)(P+Sn)\,10^4 \quad (11)$$

$$\overline{X} = (10P + 5\,\text{Sb} + 4\,\text{Sn} + \text{As})\,10^2 \quad (12)$$

The Figure 22 and 23 show relationship between increase of FATT and J Factor and $\overline{X}$ Factor at 399°C for a 3.5 percent NiCrMoV steel.
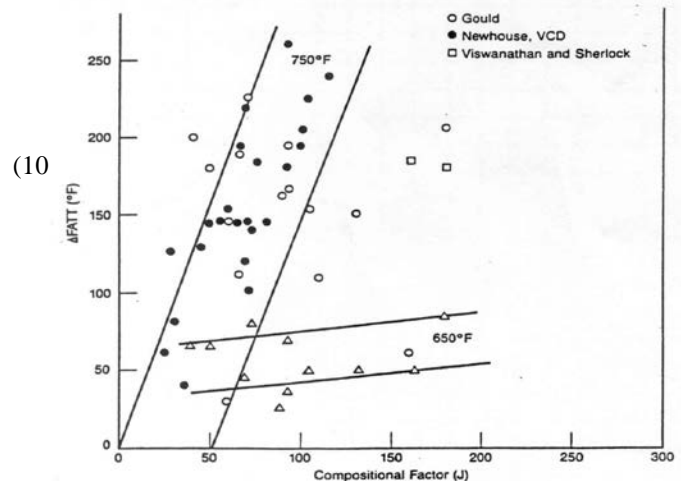

Figure 22. Correlation between compositional factor "J" and the shift in FATT of NiCrMoV Steels following exposure at 650°F and 750°F for 8800 hours.
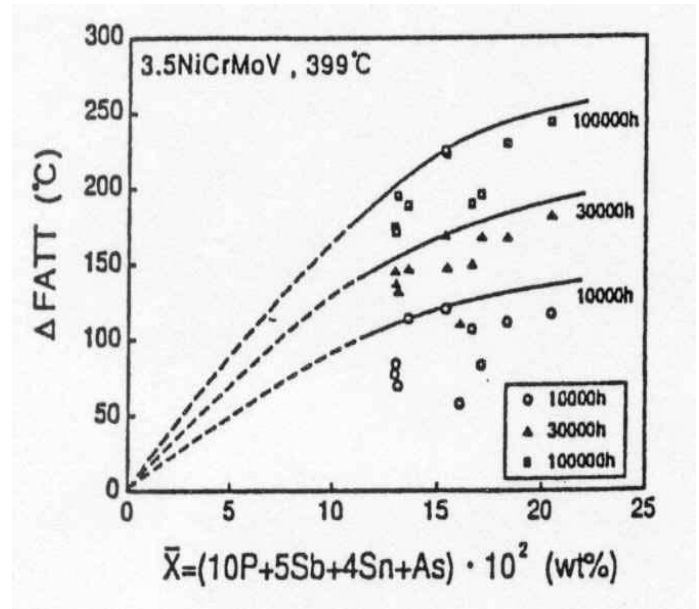

Figure 23. Relationship Between Increase of FATT and $\overline{X}$.

Small Punch Testing

Small punch testing of small disk-like specimen subjected to bending loads have found good correlation for determining the ductile-brittle transition temperature (Baik, et al. 1983). The

procedure consists of thin plate 0.4 x 0.4 x 0.02 inch is subjected to a punch deformation with a 0.09 inch diameter steel ball in a specially designed specimen holder. The test is performed at various temperatures and from the load deflector curves obtained at various temperatures, the fracture energy is calculated. The fracture energy is plotted as a function of test temperature to determine the ductile-to-brittle transition temperature. The area under the deflector curve denotes the energy absorbed during the test. This test procedure has been used successfully on a number of retired rotor samples to determine the T_{SP} (ductile-to-brittle transition) and found to correlate well with the Charpy FATT values (Foulds, et al. 1991). (Figure 24).
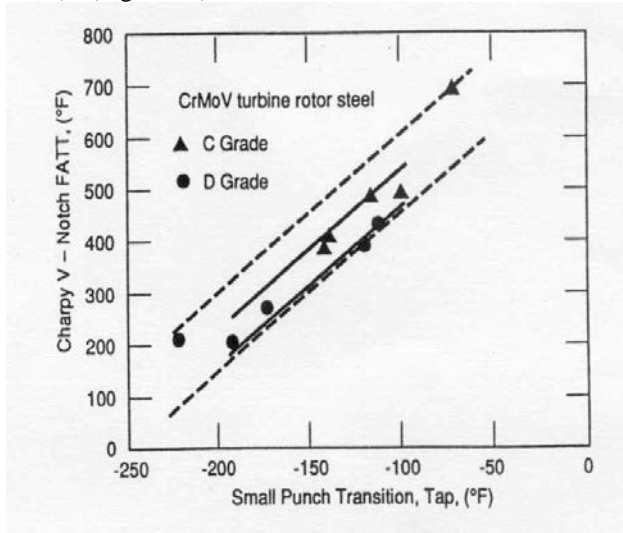

Figure 24. Correlation Between Charpy FATT and Small Punch Transition Temperature.

Chemical Etching

The grain boundaries of embrittled steel are attacked preferentially by picric acid solutions consisting of saturated picric acid solution with an addition of 1 gram of tridecyl/benzene sulfonate (per 100 ml of aqueous picric acid). Correlations have been made between the grain boundary groove depth as measured metallographically even from plastic replicas and the ΔFATT of the sample due to prior temper embrittlement. By using plastic replicas this technique becomes very attractive for field use (Kadoya, et al. 1991).

Also Kadoya, et al., was able to correlate the width of the grain boundary groove measured from plastic replicas using an SEM, with the FATT of the samples and actual rotors. They also correlated the following equation based on regression analysis of a number of material variables. This equation was found to predict the FATT within a scatter of ±20°C.
FATT = 99.12W + 1.609H_V + 816.4Si + 6520Mn + 3320P + 310.4Cr + 3404Sn + 0.282J + 325.6(13)
where:

J is defined as (Si + Mn) (P + Sn) 10^4

W = Width of grain boundary groove
H_V = Vicker Hardness of sample/rotor.

By utilizing this equation, the calculated FATT values were compared with critical FATT values and the results were very attractive (Figure 25).
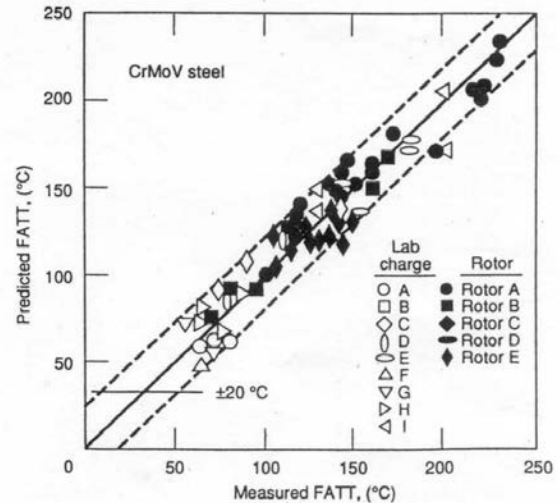

Figure 25. Comparison Between Measured FATT and Predicted FATT Using the Method of Etching.

HIGH TEMPERATURE CORROSION

Fluid catalytic cracking (FCC) hot gas expanders operate in environments that can be both corrosive and erosive. Although it is well documented that the source of erosion comes from the regenerated catalyst that is carried with the hot flue gas from the FCC, its effect on high temperature corrosion has only begun to be understood by the author's company. Papers published by the author outline the relationship of stress and temperature on the high temperature corrosion/fracture mechanics of Waspaloy in various catalyst environments (Dowson and Rishel, 1995) (Dowson and Stinner, 2000).

The nature of the corrosion attack is primarily influenced by the type of crude oil stock, which in time has a bearing on the resulting flue gas composition, regenerated catalyst and the nature and quality of additions injected into the FCC process.

When evaluating remaining life assessment of hot gas expanders especially the rotating components, one must consider the effect of the environment such as high temperature corrosion. The author's company has developed a fracture mechanics model which incorporated both the effect of oxide wedge formation and the apparent reduction in fracture toughness of Waspaloy in contact with the catalyst residue. By utilizing this model one can predict whether fracture will occur under various environmental/operating conditions of the hot gas expander. The author's company periodically tests catalysts from end-users' hot gas expanders to determine if oxide wedge can occur and what life span to reach the critical size for

failure. Generally, if the catalyst is active, then high temperature corrosion will occur. Consequently, a blade will be removed from the unit and examined metallographically to determine the oxide wedge depth. Based upon the depth and time of operation, the remaining life can be estimated, Figure 26.
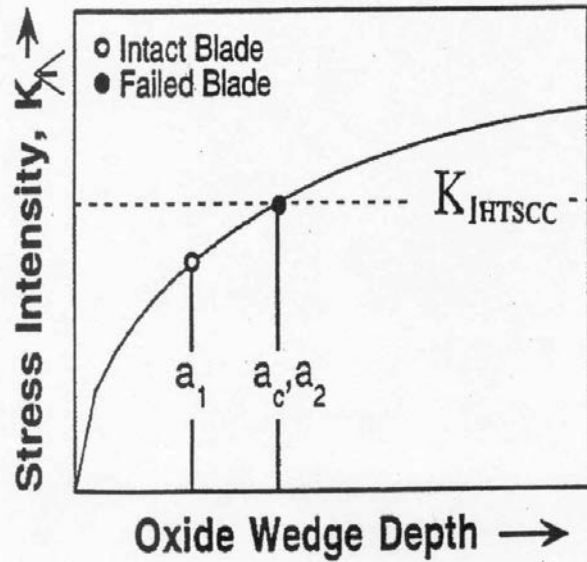

Figure 26. *Stress intensity profile vs. oxide wedge depth for unit A. Critical oxide wedge depth for failure was defined as a_c. In the failed blade, a_2 was found to exceed a_c. In an intact blade, a_1 was less than a_c.*

CASE STUDY 1 – REMAINING LIFE ASSESSMENT OF STEAM TURBINE CASING

Background Information of the Turbines

The subject ethylene plant has three steam turbines that drive three trains of compressors on the main deck. The units are listed in the following. The three turbines were commissioned in August 1981. They've been using the same steam source and are operated in similar conditions (as summarized in Table 2). This case study only discusses the remaining life assessment of one of them, a seven-stage 14 MW steam turbine.

Table 2. *Turbine Operating Conditions.*

Designed Conditions			Actual Conditions	
Temperature, °F (°C)		Inlet Pressure, psig (kg/cm²g)	Inlet Temperature, °F (°C)	Inlet Pressure, psig (kg/cm²g)
Inlet	1st Stage Disk			
806 (430)	692 (367)	696 (48.9)	797 (425)	710 (50)

According to the plant logbook, in the past 23 years, the turbine was started/stopped 24 times, which are plotted in Figure 27.
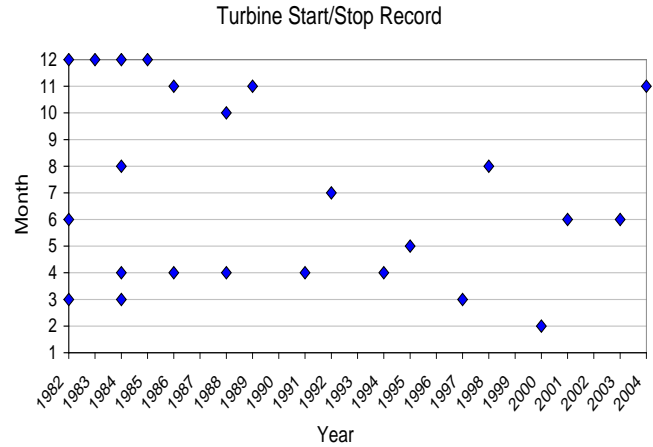

Figure 27. *Turbine Start/Stop Record.*

During the last 23 years of operation, only two failure incidents were recorded. The first one was a damage on the rotor, due to condensate inlet during the startup of the turbine in late 1980's. The other was found in the latest turnaround in 2004, in which a blade failure and multiple cracks at steam balance holes were found on 6th stage disc that was subject to repair. The casing never experienced any problem in the past. During the turnaround in 1995, a remaining life assessment was performed and the casing was found to be in a very good condition, as shown in Figure 30. The turbine component materials are listed in Table 3.

Table 3. *Turbine Component Materials.*

Steam-End Casing	Rotor Forging	Blades	Diaphragms
1.25Cr-0.5Mo alloy steel casting, ASTM A217 Grade WC6 (limited to 950°F service)	Ni-Mo-V alloy steel, ASTM A470 Class 4	AISI 403 stainless steel for all stages	Alloy steel plate ASTM A517 Grade F & A516 Grade 60 for 2nd to 5th stages. Gray cast iron ASTM A278 Class 40 for 6th & 7th stages.

Field Inspection

The turbine upper casing was visually examined. No cracks or reportable indications were found. The split-line bolt-holes were examined with dye-penetrant inspection, which did not reveal any cracks. The casing was polished at six different spots shown in Figure 28. The microstructure was observed with a portable optical microscope, and replicated for documentation (Figure 29). Microstructure deteriorations, such as carbide precipitation at grain boundaries and bainite degradation, were evident. However, the casing did not show any creep voids at any of the spots being examined. Hardness was measured at the

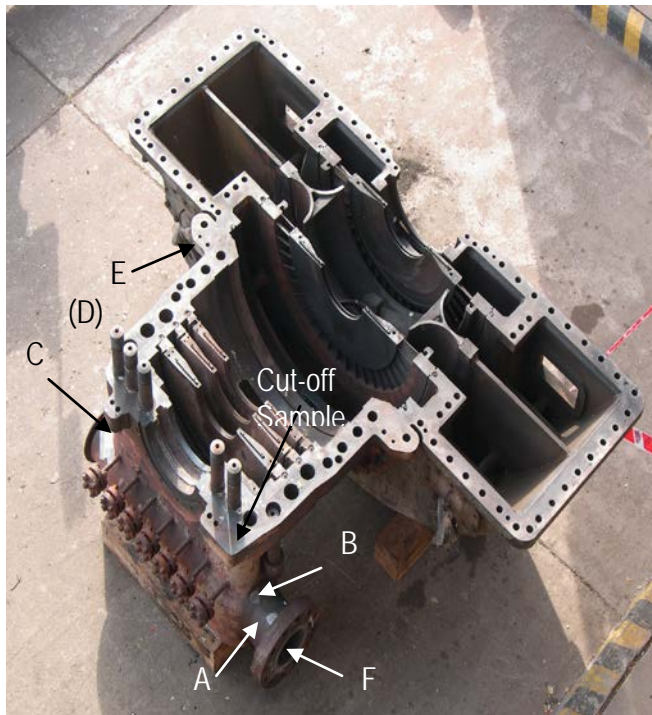same spots and the results are listed in Table 4.

Figure 28. The turbine casing and the replication/cut-off locations. F represented the hottest spot, while E represented the coolest spot. D was at the transition radius of steam chest to casing barrel, which was invisible from this photo.
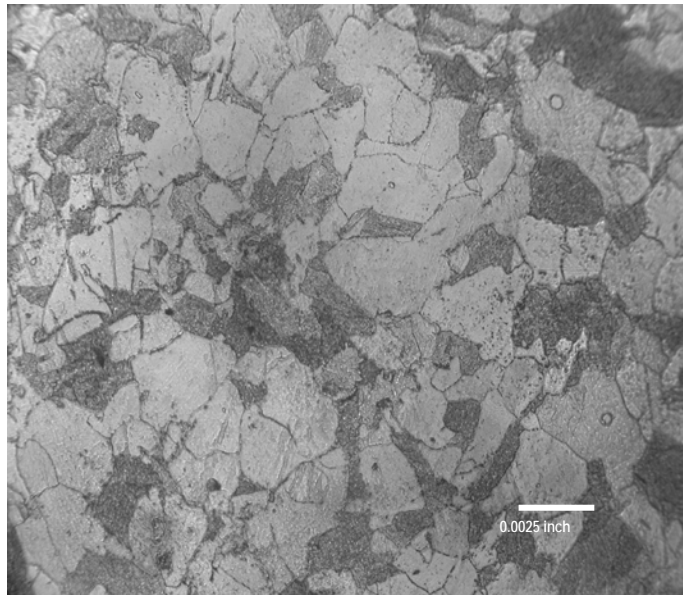

Figure 29. Micrograph of a replica taken from spot D. Carbides precipitated and partially networked at grain boundaries. However, no creep voids were observed there. 5% Nital etched.

Table 4. Casing Hardness was Consistent from Spot to Spot.

Spot ID#	Brinell Hardness [HB] (converted from Equotip data)			
	1st Reading	2nd Reading	3rd Reading	Average
A	152	150	155	**152**
B	151	151	156	**153**
C	154	151	153	**153**
D	159	158	159	**159**
E	137	141	140	**139**
F	154	154	154	**154**

Microstructure Deterioration of the Casings Material

In order to study the microstructure deterioration, a fragment of the sample being cut-off from the casing was reheat treated to restore the original microstructure for comparison. The reheat treatment was done in two steps: normalized at 1685°F (918°C) for 1 hour and controlled air-cool, then tempered at 1250°F (677°C) for 2 hrs and air-cool. The controlled air-cool from austenite temperature was to obtain a similar percentage ratio of proeutectoid ferrite and bainite as of the original heat treatment. Assuming the casting was 2–3/4 inch (70 mm) thick, a cooling rate of 54°F per minute (30°C/m) was employed and the resulted ferrite/bainite ratio simulated the original heat treatment very well.

The reheat treated and service-exposed samples were mounted and polished and examined with optical and scanning electronic microscopes (SEM). Their hardness was also measured. The findings are summarized in the following.

- Comparing with the restored microstructure, the service-exposed samples showed profound carbide precipitation at grain boundaries and the extent of the precipitation increased with increasing the service exposure time (Figure 30).
- Service-exposed samples also showed carbide precipitation inside the proeutectoid ferrite phase.
- Evidence of microstructure degradation of the bainite phase was noticed in the service-exposed sample, due to the transformation of cementite (M_3C) into different carbides (M_2C & M_7C_3).
- No creep voids were found in either sample.
- Hardness was measured as HRB 91 (HB 160) for service-exposed sample and HRB 93.5 (HB 169) for reheat treated sample, indicating a slight hardness decrease after a long-term exposure at elevated temperature.

Figure 30. The service-exposed sample(Top) showed partially networked carbides at grain boundaries and degradation in bainite (dark phase), comparing with the reheat treated (restored) microstructure. It can also be seen that carbides precipitated inside the proeutectoid ferrite (white phase) in service-exposed condition. 5% Nital etched.

Discussion & Conclusions

Turbine casings usually are normalized and tempered after being cast. This heat treatment leads to a desirable combination of strength/hardness and toughness/ductility for the casing material, 1.25Cr-0.5Mo alloy steel in this case. It also gives an excellent thermal stability for the casings. The typical treatment process contains normalizing at 1685°F (918°C) followed by air-cool then tempering at 1250°F (693°C) followed by air-cool.

The microstructure after the heat treatment consists of proeutectoid ferrite plus bainite. Bainite is a metastable aggregate of ferrite and cementite, which may degrade after long-term exposure at elevated temperature. The degradation was observed as a transformation of cementite (M_3C) into M_2C and M_7C_3 carbides (Biss and Wada, 1985). This transformation will lead to less carbides (in volume percentage) and coarser carbide particles, which will result in lower strength and hardness, which may reduce fatigue and rupture strengths of the material.

Carbon will also diffuse along the grain boundaries and into the proeutectoid ferrite phase to form carbides. Carbides at grain boundaries, especially in networked form, are considered detrimental because they can result in embrittlement and reduce rupture ductility of the material. Another grain boundary damage that is also related to long-term diffusion but was not seen in this case is creep voids. Creep voids are considered as a higher-degree of microstructure damage than the carbide precipitation, and a warning sign of component remaining life. In the subject turbine casing, no creep voids were evident yet, so the microstructure deterioration was considered moderate and not immediately harmful to the casing life. It was concluded that the casing could be safely used for the following service period (about 5 years). However, the microstructure deterioration imposed a concern of the integrity of the casing material and consequent potential risks on the creep strength and rupture ductility of the casings. It was reported that 1.25Cr-0.5Mo low alloy steel could lose its rupture ductility after long-term exposure at elevated temperature (Demirkol, 1999). This behavior is so called Rupture Ductility Trough, which is related to carbides precipitation and may occur before creep voids are developed.

Therefore, in addition to continually monitoring the microstructure with non-destructive replica techniques in next turnaround, the authors' company suggested the ethylene plant to conduct a Level III Remaining Life Assessment, which requires destructive material tests, in order to evaluate the extent of damage on creep strength and rupture ductility of the casing material. The material tests mainly consist of SRT (stress relaxation test) and CDR (constant displacement rate) test, which are described in previous section. These two mechanical testings can supply information that microstructure examination (replica) cannot.
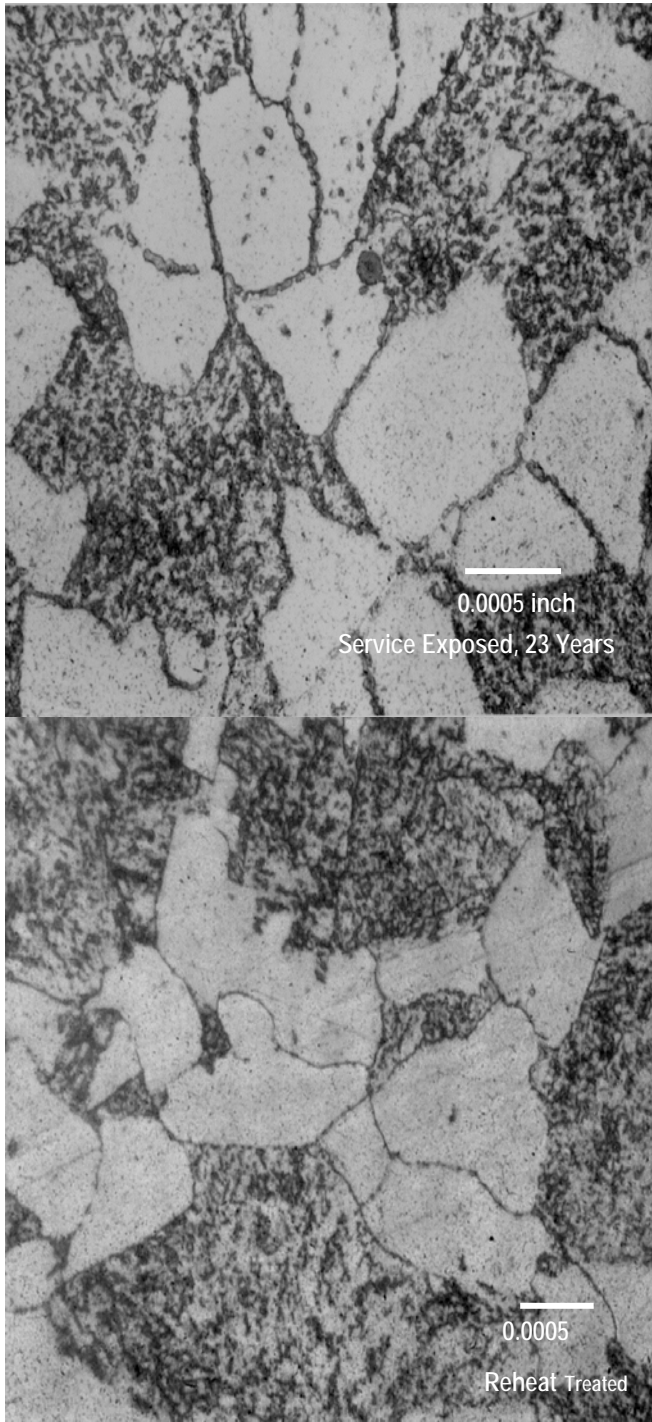
CASE STUDY 2 – REMAINING LIFE ASSESSMENT OF STEAM TURBINE ROTOR

Background

The author's company was asked by the end user to assist them in the assessment of the remaining life of a 44 MW H.P. steam turbine. The objective of the assessment was to propose recommendations on the steam turbine's rotor reuse and long term serviceability. This was a Westinghouse steam turbine that has operated for 50+ years at inlet conditions 950FTT and 1250 PSIG.

Field Inspection of HP Rotor

The rotor was NDE (Non-Destructive Examination) inspected, using a liquid fluorescent inspection method, which revealed no obvious indications. During the course of the NDE inspection the blades were not removed. Therefore no comment was made regarding the service condition of the disk roots on the rotor. A borosonic inspection inside of the shaft bore was performed which revealed two significantly large indications. Both these indications were machined out and the follow up borosonic inspection confirmed that both had been removed.
The rotor was polished at higher (inlet) and lower (exhaust) temperature locations (Figure 31). Each location was etched and replications were taken to observe the rotor's microstructure under an optical microscope (Figures 32-35). Microstructural deteriorations, such as carbide precipitation at grain boundaries and bainite degradation, were evident. However, the rotor did not show any creep voids at any of the locations being examined. Positive Material Identification (PMI) analysis indicated that the material was a Ni-Mo-V turbine rotor steel (ASTM A470 Cl. 4).

Microstructure Deterioration of the HP Rotor Material

➤ Metallurgical examination of the rotor's microstructure revealed evidence of degradation of the bainite phase of the material due to its long service at approximately 950°F.
➤ Evidence of microstructure degradation of the bainite phase was observed in the replicas, due to the transformation of cementite (M_3C) into different carbides (M_2C and M_7C_3).
➤ Microstructural degradation was significantly less at the last stage due to much lower operating temperatures at this location.
➤ The microstructural degradation is best illustrated by comparing virgin rotor steel with the replicas from the in service steel (Figures 36).
➤ No creep voids were evident.
➤ Hardness measurements taken at the inlet and exhaust areas of the rotor were found to be approximately 22 HRC respectively. The expected hardness value of non-service

Ni-Mo-V turbine rotor steel is approximately 25HRC maximum. This represents a relatively small hardness decrease considering the rotor's long-term exposure at elevated temperatures. However a decrease in hardness indicates that the creep strength of the material has deteriorated.
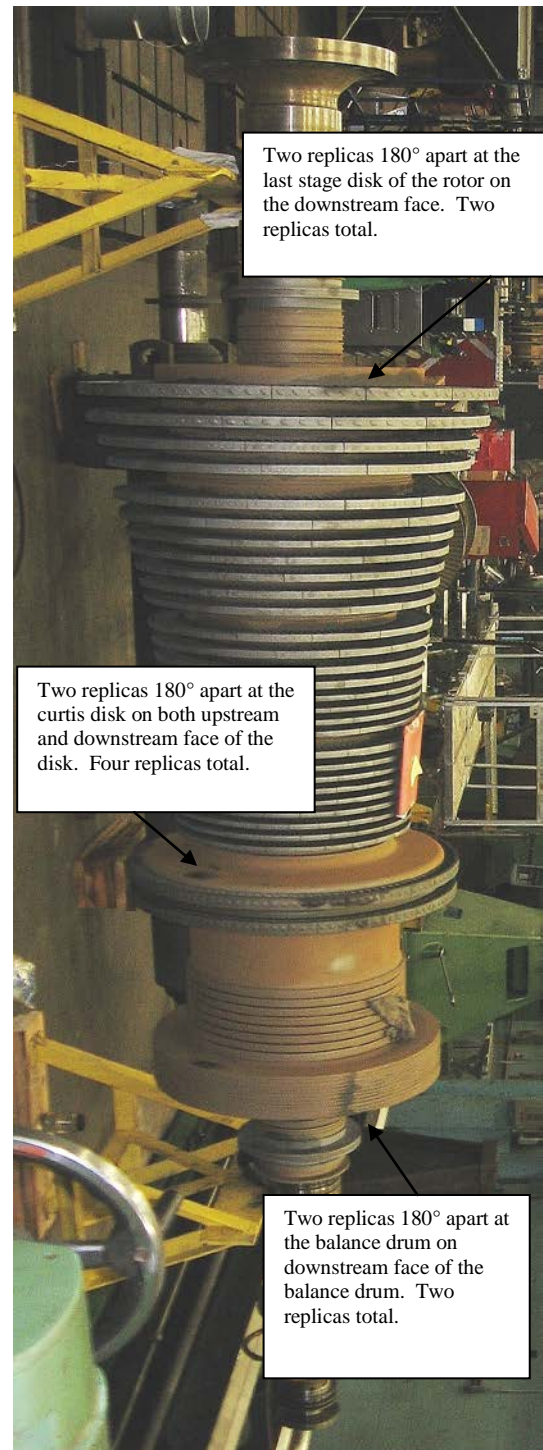

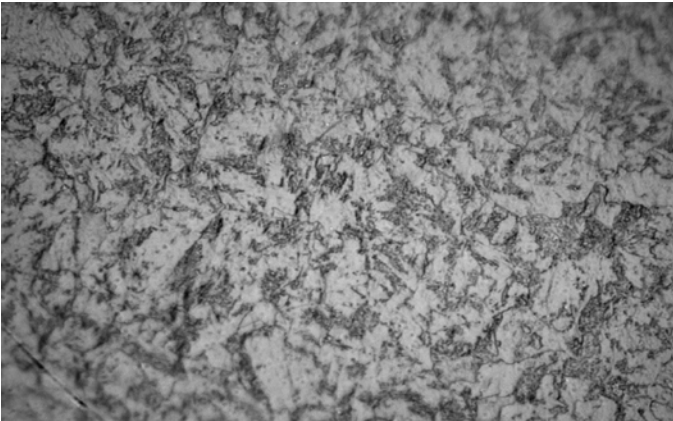*Figure 31. Areas of Metallographic Replication*

Figure 32. Metallographic Replica, on the Downstream Face of the balance drum, Showing Slight Bainite Degradation Due to Prolonged High Temperature Service. Etched in 5% Nital. 200X
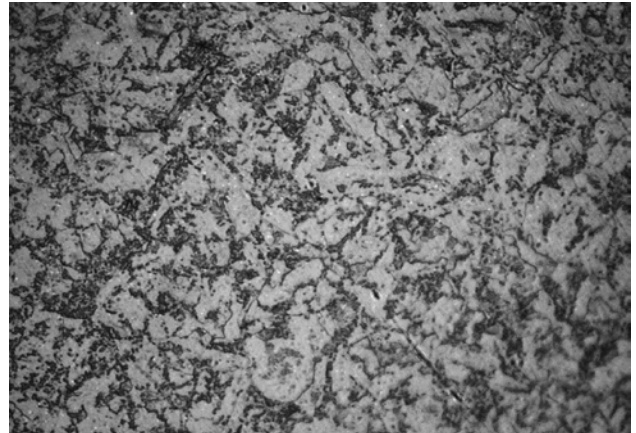

Figure 35. Metallographic Replica, on the Downstream Face of the Last Stage Disk, Showing Less Degradation When Compared to the High Temperature Locations. Etched in 5% Nital. 200X
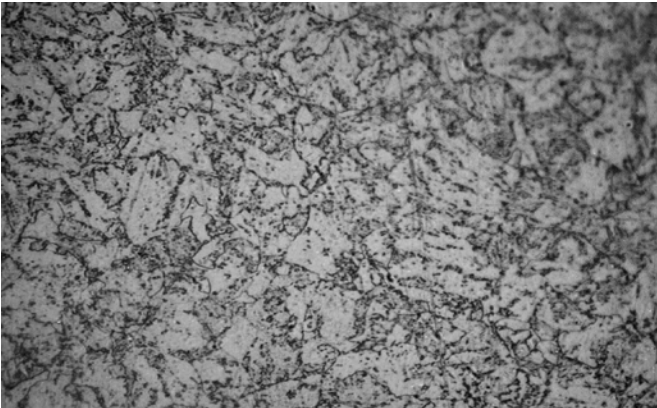

Figure 33. Metallographic Replica, on the Upstream Face of the Curtis Disk, Showing Slight Bainite Degradation Due to Prolonged High Temperature Service. Etched in 5% Nital. 200X

Figure 34. Metallographic Replica, on the Downstream Face of the Curtis Disk, Showing Slight Bainite Degradation Due to Prolonged High Temperature Service. Etched in 5% Nital. 200X
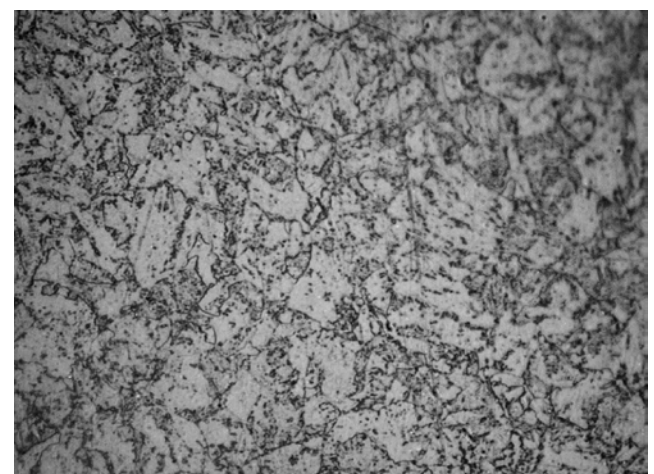
Figure 36. Comparing virgin Ni-Mo-V rotor steel (top) and the replica of the upstream face of the curtis disk taken from the service rotor steel. The degradation of the bainite phase is observed due to the transformation of cementite (M_3C) into different carbides (M_2C and M_7C_3).
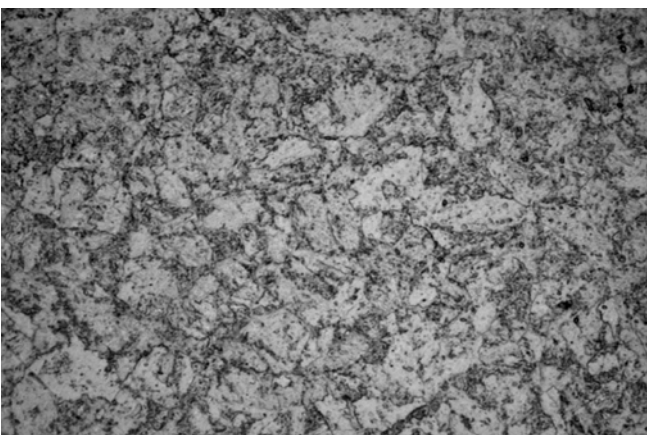
Discussion and Conclusions

Metallurgical examination of the rotor's microstructure revealed evidence of degradation of the bainite phase of the material due to its long service at approximately 950°F. Bainite is a metastable aggregate of ferrite and cementite, which may degrade after long-term exposure at elevated temperatures. The degradation was observed as a transformation of cementite (M_3C) into M_2C and M_7C_3 carbides. This transformation leads to less carbides and coarser carbide particles, and results with lower strength and hardness, and reduces the ductility of the material.

Carbon will also diffuse along the grain boundaries and into the proeutectoid ferrite phase to form carbides. Carbides at grain boundaries, especially in networked form, are considered detrimental because they can result in embrittlement and reduce rupture ductility of the material.

Another grain boundary damage mechanism that is also related to long-term diffusion but was not seen in this case are creep voids. Creep voids are considered a higher degree of microstructure damage than carbide precipitation, and a warning sign of reduced component remaining life. In the HP rotor, no creep voids were evident yet, so the microstructure deterioration was considered moderate and not immediately harmful to the rotor life. It is concluded that, with respect to creep damage, the rotor is in undamaged (no creep voids) condition. It is recommended the rotor's microstructure be re-evaluated after 5 years.

CASE STUDY 3 – REMAINING LIFE ASSESSMENT OF HOT GAS EXPANDER DISK AND BLADES

A life assessment was performed on a TH140 power recovery unit for both the disk and rotating Waspaloy blades. The unit had been in continuous operation for 10 yrs, accumulating approximately 85,000 hrs. The operational data revealed that the unit has run with a inlet temperature of 1296°F with only one afterburn where the temperature reached 1476°F for 3 days. This life assessment consisted of:

a) Testing of modified stress rupture specimens in the pressure of FCC unit catalyst in order to determine if the species trapped in the catalyst were hazardous to the expander disk and blades.
b) Corrosion testing
c) Perform microstructural evaluation of both the disk and blades root locations using replication technique
d) Hardness reading at both blade and disk root at both inlet and exhaust faces.
e) Two blades were destructively tested to perform stress rupture, stress relaxation testing, constant displacement rate testing and evaluate evidence of high temperature corrosion attack. One of the blades was resolutioned and aged so that the results could be compared against the blade in the serviced condition. The blades removed from the disk were the original blades and had seen approximately 85,000 hrs.

a)   Catalyst Corrosion Testing

In the present investigation a number of tests were done at stress levels of 75 ksi and at a temperature of 1350°F. Results varied with some bars failing before 5 hrs while others did not. Four Waspaloy rupture specimens W1-W4 were tested. Two failed while the other two did not (Table 5).

Table 5. Results of Catalyst Corrosion Testing

Specimen ID	Catalyst	Load (Mpa)	Temp. (°C)	Duration (hours)	Status	Failure Location	Failure Mode	Fracture Morphology	Corrosion Wedge
W1	C1 (V-17)	482.6	700	0.67	Failed	notch	corrosion - rupture	intergranular	Yes
W2	Air	482.6	700	100	Intact				No
	C3 (V-17)	482.6		30	Intact				No
	C5 (V-66)	482.6		0.12	Failed	notch	corrosion - rupture	intergranular	Yes
W3	C5 (V-66)	482.6	593	5	Intact	This specimen was sectioned for evaluation			No
			700	5	Intact				No
			700	24	Intact				No
W4	C6 (V-66)	482.6	700	18	Intact	This specimen was not sectioned for evaluation			
				17.5	Intact				
				6.5	Intact				
	C5 (V-17)			23	Intact				
	C3 (V-17)			21	Intact				

Both W1 & W2 fractures were examined using a scanning electron microscope (SEM) and the morphology was found to be intergranular for both fractures (Figures 37-39). Corrosion wedges were found on the surface at the notch of both specimens (Figure 40).
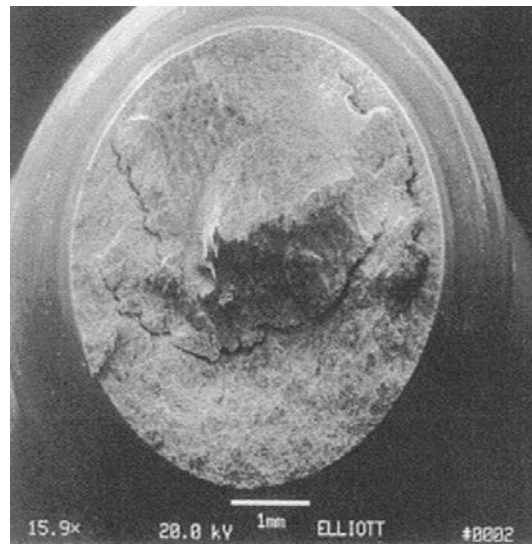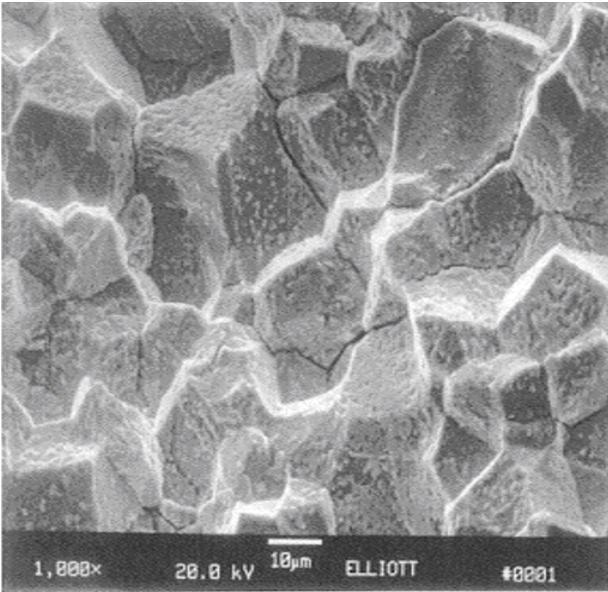

Figure 37. of Specimen W2

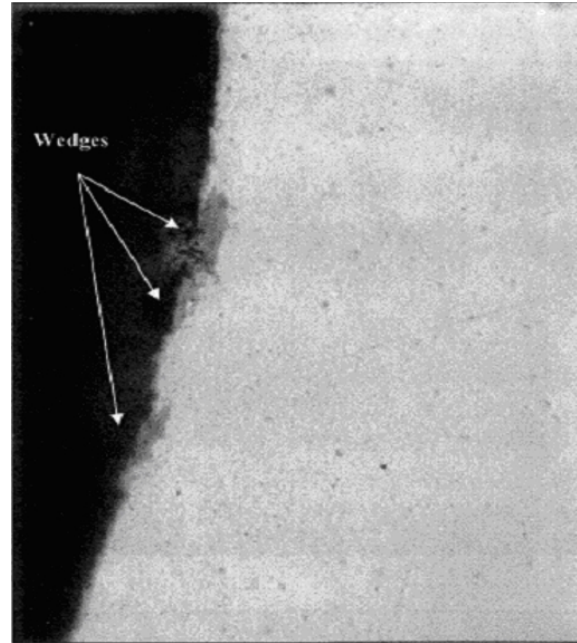Figure 38. SEM of Specimen W2 with dominant intergranular feature

Figure 40. Cross-section of specimen Note the sulfidation corrosion wedges found on the notch surfaces where the stress was concentrated.

SEM/EDS indicated that the corrosion product was sulfide. This sulfide evidence is a strong indication of high temperature sulfidation corrosion. Figure 41 shows setup for catalyst test.
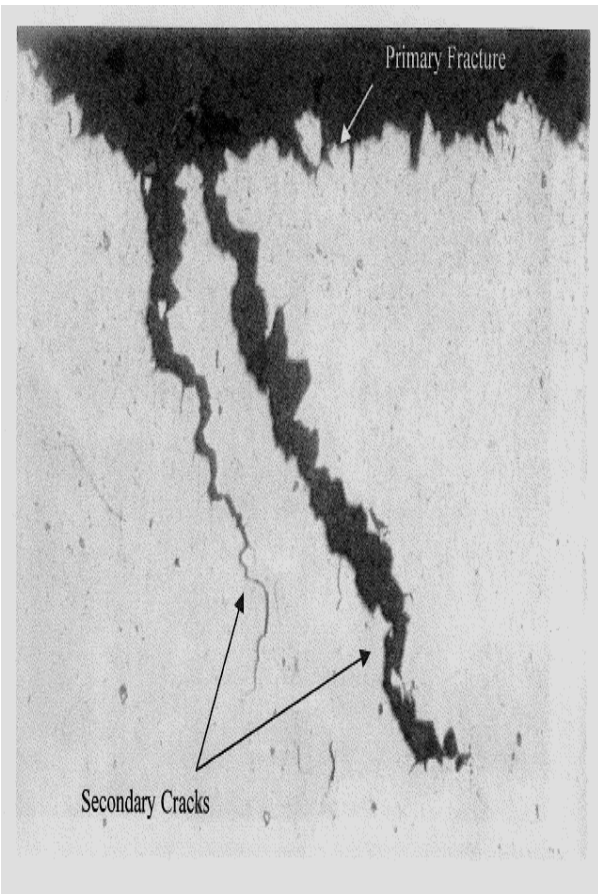

Figure 41. Setup of Stress-Rupture Rig for Catalyst Testing

Figure 39. Cross-section of the fracture of specimen W2. Intergranular secondary cracks, located near the center of axis, were evident.
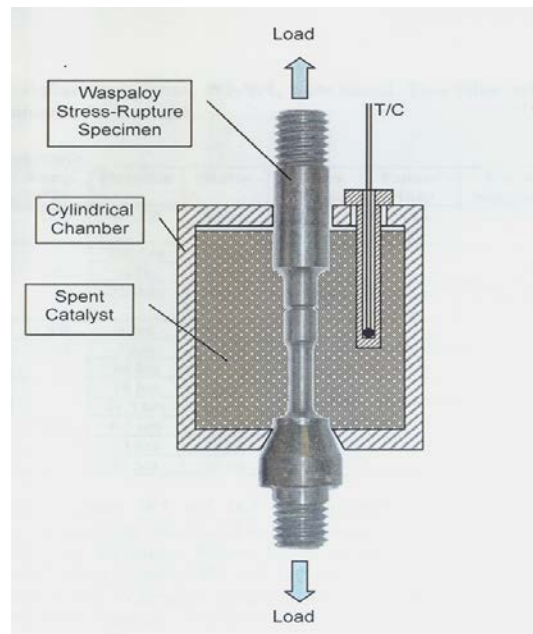
Since the results were inconclusive that the spent catalyst was contaminated further destructive tests were performed in the blades such as SRT and CDR.

b) Corrosion Testing

The depth of the corrosion product was measured by taking cross-sectional samples along the top inside radius of the blade root. The five samples were mounted and polished for examination under an optical microscope. Corrosion wedges, as seen in Figure 42 were found along this inside radius. The deepest corrosion wedge found at any location along this inside radius is shown in Figure 42, and depth of the corrosion wedge is 0.0043 inches (4.3 mils).
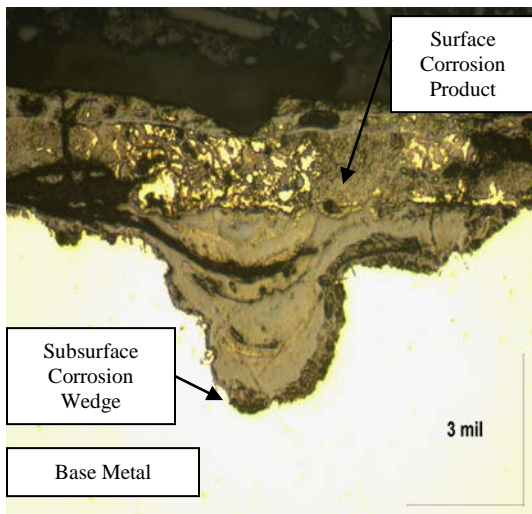

Figure 42. Photomicrograph of deepest corrosion wedge found in the blade root

Using a Scanning Electron Microscope (EDS), Energy Dispersive Spectroscopy (EDS) was performed on the corrosion product. The results of the EDS analysis indicate that the corrosion product on the surface of the Waspaloy is Nickel Oxide and Nickel Sulfide while the subsurface corrosion product is Chromium Oxide and Chromium Sulfide. These corrosion products are common in Nickel-based alloys which are under stress in environments containing both Oxygen and Sulfur.

The rate controlling operation in the high temperature corrosion process on the disk roots is the diffusion of ions through the oxide layer that has formed. When diffusion is the rate controlling step, the depth of the corrosion wedge will increase at a parabolic rate determined by the equation below.

Equation: $$X^2 = [\,k_p * t\,]\,/\,2$$

In this equation, X is the depth of the corrosion wedge, t is the time, and k_p is the parabolic rate constant. Knowing the maximum corrosion wedge depth is 4.3 mils after approximately 85,000 hours of operation, the constant k_p for this equation is 4.35×10^{-4} mils^2/hour.

c) Hardness Testing

Hardness readings were taken on both the inlet and exhaust faces of the disk root (Table 6). The hardness readings were consistent at all locations on both faces of the disk and met the requirements of the authors' Waspaloy material specification. This evidence indicates that the disk material had not been exposed to excessive heat during operation.

Table 6. Average Hardness Values at Examined Disk Locations

	Inlet Face	**Exhaust Face**
Tip of Disk Root	37.7 HRC	38.2 HRC
Base of Disk Root	39.4 HRC	40.9 HRC
Disk Body	39.8 HRC	40.1 HRC

d) Microstructural Evaluation

Replicas of the microstructure of the disk were taken from disk root locations shown in Figure 43 and subsequently examined by an optical microscope. The replicas were a rubber like resin substance attached to backing paper. The microstructures of the replicas and are consistent at all locations on both the inlet and exhaust faces of the disk. The average grain size at all locations on the disk is ASTM 5.5 and conforms to the requirements of the authors' Waspaloy material specification. This is further evidence that the disk material was not exposed to excessive heat during operation. The microstructure indicated there was not evidence of creep damage as there were no voids at the grain boundary triple points (Figures 44-46).
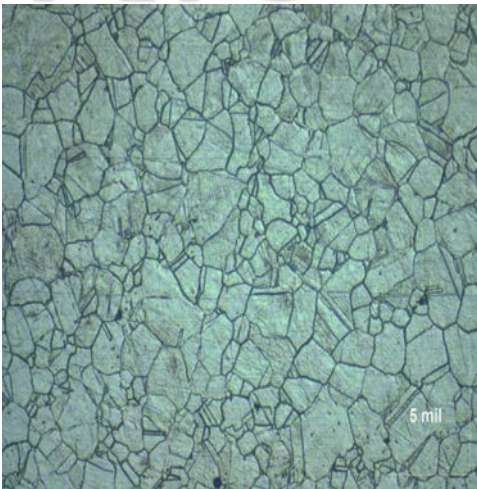

Figure 43. Diagram illustrating the locations of the disk from which replicas were taken. Areas were examined on both the inlet and exhaust faces of the disk
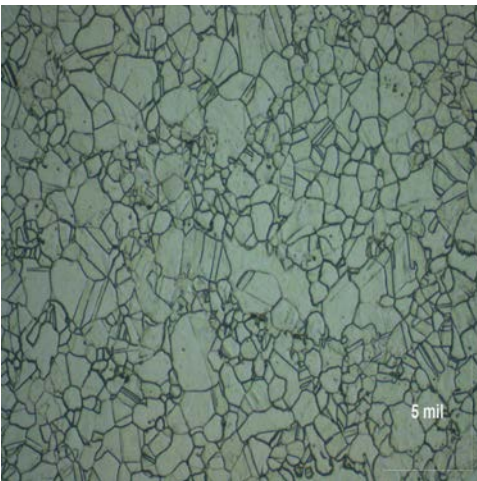
Figure 44. Inlet Face – Tip of Disk Root.
Photomicrograph taken from Replica

Figure 45. Exhaust Face – Tip of Disk Root.
Photomicrograph taken from Replica

Figure 46. Inlet and Exhaust Face.
Photomicrograph taken from Replica.

e) Blade Examination

Two of the Waspaloy blades that had seen 85,000 hrs were taken out of service for destructive testing. One of the blades was resolution treated and aged in accordance to the authors' Waspaloy heat treatment procedure and sectioned for mechanical and metallurgical examination. The other blade referred to "as service condition" was tested in a similar manner to the reheat treated blade.
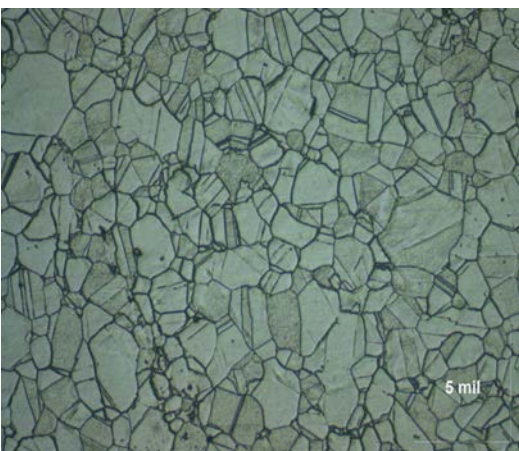
Sections from the root of the "as service condition blade" and the "reheat treated blade" were sectioned and polished for examination under an optical microscope. Photomicrographs of the microstructure of these blade roots are shown in Figures 47 & 48. The photomicrographs show that the average grain size of both blade roots is ASTM 4 which is slightly larger than the average grain size of the disk, however, this grain size still meets the authors' material specification requirements. Again, no evidence of creep damage or exposure to temperatures beyond the designed service temperature could be found.
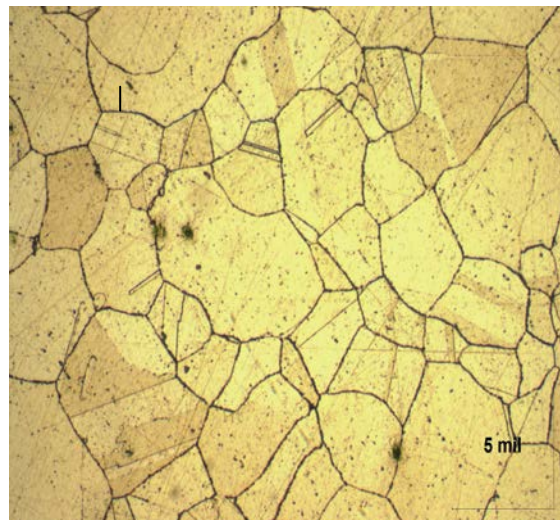

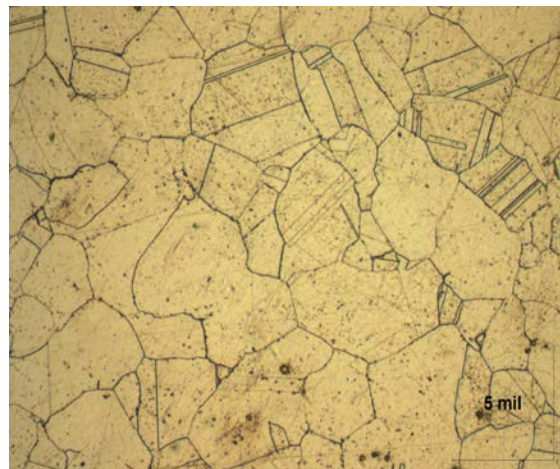*Figure 47. Photomicrograph of Service Condition Blade Root*

Figure 48. Photomicrograph of Re-Heat Treated Blade Root

There is a slight difference between the grain boundaries of the as-serviced blade and the re-heat treated blade under higher magnification. The grain boundaries of the service condition blade, shown in the photomicrograph in Figure 49, reveal that the grain boundaries are not completely discrete at all locations. There is also evidence that carbides are precipitating at the grain boundaries. These observations are illustrated by comparison to the microstructure of the re-heat treated blade, which is shown in the photomicrograph in Figure 50. The grain boundaries of the re-heat treated blade are more discrete and there are fewer precipitates present at the grain boundary locations.
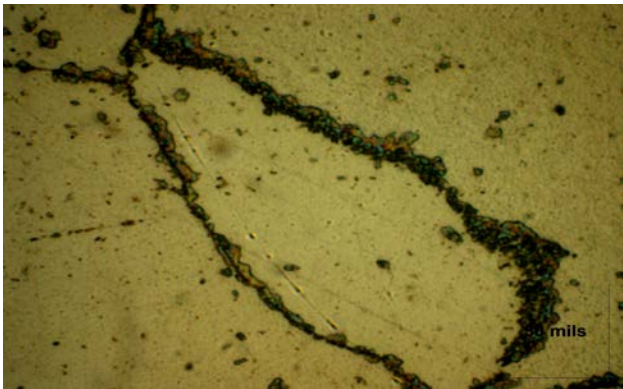

Figure 49. Photomicrograph of Grain Boundary on Service Condition Blade Root
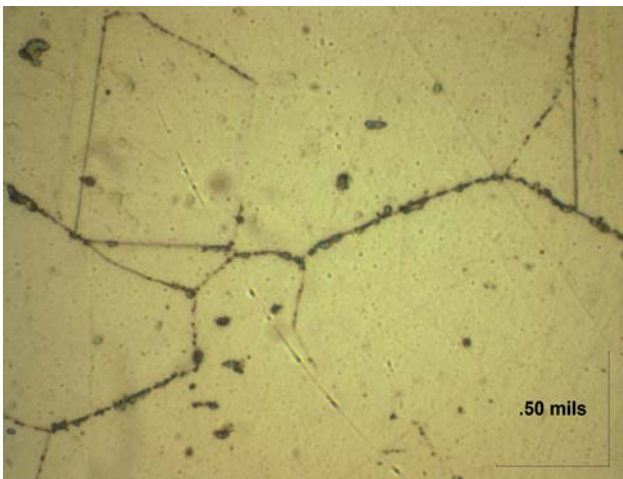

Figure 50. Photomicrograph of Grain Boundary on Re-Heat Treated Blade

Stress Rupture Testing

Stress rupture testing was performed on samples taken from service condition blades as well as the reheat treated blade root. The stress rupture bars were standard smooth/notch bars in accordance with ASTM E292 specimen #4. The results of the stress rupture testing are shown in Table 7.

Table 7. Stress Rupture Testing Results

Stress Rupture Testing 1350°F at 75,000 psi stress			
	Time to Fracture	% Elongation	Fracture Location
Service Condition Blade	40.44 hours	23%	Smooth
Reheat Treated Blade	70.34 hours	9%	Smooth

Stress Relaxation Testing (SRT) and Constant Displacement Rate Testing (CDR)

The traditional approach to creep design involves long time testing and incorporates microstructural evolution in the test measurements. Stress relaxation tests (SRT) and constant displacement rate (CDR) tests can be used to evaluate these microstructural changes in samples which have been exposed to service conditions. For determination of the creep strength in a short time testing, a stress vs. creep rate response is determined from an SRT test and the fracture resistance can be determined from a CDR test.

Creep Strength Evaluation

As previously mentioned, the creep rate data can be determined from an SRT test. A strain is placed on the specimen and is held constant, and the stress in the specimen relaxes as the elastic strain is replaced by inelastic creep strain. At a constant strain, the creep rate of the sample is equal to the total strain minus the elastic strain. The stress vs. time response during relaxation may be differentiated and divided by the elastic modulus to give the creep rate, which can then be plotted against the stress. By comparison to standard results, changes in state induced by heat treatments or service exposure can be evaluated.

Fracture Resistance Evaluation

CDR testing may be used as a means to accelerate the development of notch sensitivity found in long time creep rupture testing of notched samples. The CDR testing of a notched sample can be used for fracture resistance evaluation in this short time test at temperatures and strain rates where the alloy is most vulnerable to fracture. The constant displacement rate across the notch ensures that once a crack initiates, the crack will grow under control until a critical crack length for brittle fracture is exceeded. The displacement at the time of failure and the extent of unloading at failure provide measures of the fracture resistance of the alloy.

Experimental Procedure and Results

Standard tensile specimens taken from both the service condition blade and the re-heat treated blade were taken. The SRT test specimens had a 1 inch gauge length and were 0.160 inches in diameter. The CDR test specimens had the same dimensions with a 60° notch in the center of the gauge length. The test matrix is given below. Samples tested under similar conditions, such as SRT 1 and SRT 4, were taken from identical locations in both the service condition blade and the re-heat treated blade (Table 8).

Table 8

Service Condition Blade	
SRT 1	SRT from 0.4% total strain and 1.3% total strain at 600°C
SRT 2	SRT from 0.4% total strain and 1.3% total strain at 700°C
SRT 3	SRT from 0.4% total strain and 1.3% total strain at 800°C
CDR1	600°C
CDR 2	650°C
Re-Heat Treated Blade	
SRT 4	SRT from 0.4% total strain and 1.3% total strain at 600°C
SRT 5	SRT from 0.4% total strain and 1.3% total strain at 700°C
SRT 6	SRT from 0.4% total strain and 1.3% total strain at 800°C
CDR 3	600°C
CDR 4	650°C

The strain levels of 0.4% total strain and 1.4% total strain were selected to so that the SRT tests would be conducted just beyond the elastic limit of the material and at a plastic strain of 1%. This testing produces comparative relaxation data for the unrestrained condition at 0.4% total strain and a comparison basis with long time creep data to 1% creep strain at 1.4% total strain.

The test procedure involved loading the SRT tests to the prescribed strain levels and holding at that strain for 20 hours at temperature. During the holding time, the stress relaxes as the elastic strain is replaced with inelastic creep strain. After holding for 20 hours, the stress on the samples was reduced to approximately 1.5 ksi and held constant for 2 hours while the samples contracted due to recoverable time-dependant anelastic strain. The stress at various times during the relaxation of the samples was recorded.

Using the elastic modulus of the material which was measured during the loading of the test, the stress vs. time response was fitted with a fourth order polynomial which was differentiated to convert to a stress vs. creep rate curve. The data obtained from this testing covers approximately five decades of time. From the stress vs. creep rate curves, the time required to induce 1% creep on the material was calculated. Using the estimated times for 1% creep, a Larson-Miller parameter curve was constructed. This curve is shown in Figure 51. The Larson-Miller curves again demonstrate the slight reduction in creep strength of the service-condition material in comparison to the re-heat treated material for the 600°C and 700°C samples.
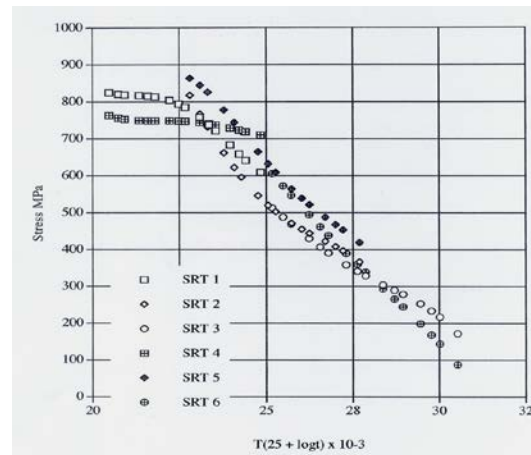

Figure 51. Stress vs. Larson Miller Parameter for 1% Creep of Service Condition Blade and Re-Heat Treated Blade

Figure 52 gives a comparison of the creep rate curves at various stresses for both the re-heat treated material and the service condition material against standard Waspaloy samples. As seen in Figure 52, although the creep rate curves of the service condition material is lower than that of the re-heat treated material, the creep rate curves of the service condition material is approximately the same as the standard Waspaloy samples at 600°C and 700°C and even higher than the standard samples at 800°C.
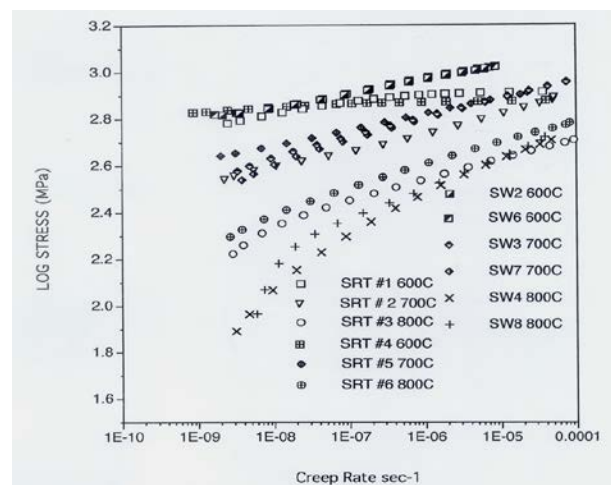

Figure 52. log Stress vs. Creep Rate Curves Comparing the Service Condition Blade and the Re-Heat Treated Blade with Standard Waspaloy Samples

The test procedure for the CDR specimens involved heating the samples to 600°C and 650°C because Waspaloy material displays a ductility minimum at these temperatures. A constant displacement rate of $7x10^{-5}$ mm*sec^{-1} was then applied. The displacement across the notch at the time of fracture and the amount of unloading before the fracture both give a measurement of the fracture resistance of the material. Stress readings were taken at 1 second intervals for these tests, and the amount of unloading recorded is a measure of the crack size prior to fast fracture. The results of this testing for both the re-heat treated samples and the service condition samples are given in Figure 53.
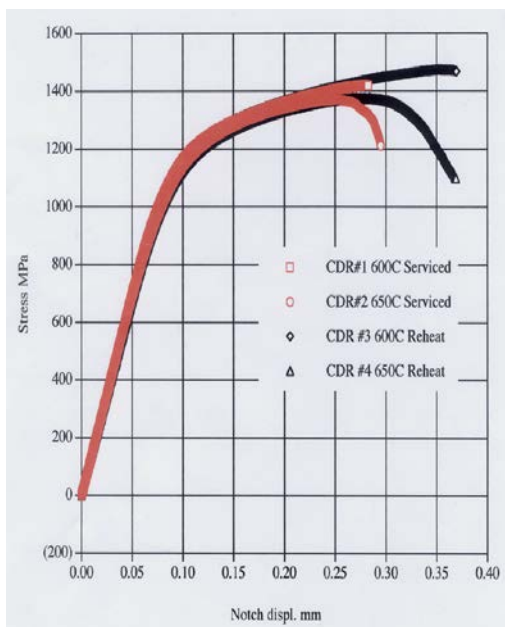

Figure 53. CDR Results at 600°C and 650°C for Service Condition Blade and Re-Heat Treated Blade

It is clear from the results in Figure 27 that the re-heat treated material has significantly greater notch displacement at the time of fracture than the service condition material at both testing temperatures. The re-heat treated material also demonstrated a much greater amount of unloading at 650°C than the service condition material. The notch displacements of the re-heated material were comparable to standard Waspaloy samples. Although the service condition material has less notch ductility than the re-heat treated material, stress rupture testing indicated that the service condition material is not notch sensitive as the stress rupture sample fractured in the smooth location.

Remaining Rupture Life

From the data generated during the Stress Relaxation Testing, a graph of Stress vs. Time to 1% Creep was obtained and is displayed in Figure 23. This graph provides stress

rupture data from the service condition material and can be used to determine the remaining stress rupture life of disk.

The SRT testing of the service condition material was performed at 600°C, 700°C and 800°C, yielding Stress vs. Predicted Time to 1% Creep data at these three temperatures. The average inlet temperature of the unit was reported to be 1297°F (702°C). Using the SRT data for the service condition material at 700°C in Figure 23 along with a very conservative value for the mean stress at the disk root, the disk will reach 1% creep after $3x10^6$ hours of operation. This disk has currently experienced 85,000 hours of operation, which is only 3% of the 1% rupture life. Since this calculation was based on the inlet temperature of the unit, the time to 1% creep is an extremely conservative value because the disk root will be exposed to lower temperatures than the inlet temperature.

Only one significant afterburn was reported by the customer, where the inlet temperature of the expander reached 1467°F (797°C) for 3 days. By using the Stress vs. Time to 1% Creep data in Figure 21 for the service condition material tested at 800°C and using the same conservative mean stress value at the disk root, a time of 2,340 hours is necessary before the disk experiences 1% creep deformation. The disk may have seen this temperature for up to 72 hours, which equals 3% of the 1% rupture life under these conditions. Again, this is a very conservative value since the expander disk root will be exposed to a lower temperature than the inlet temperature. By using the Life Fraction Rule which states the fraction of the remaining rupture life used up under various conditions may be added up to determine to total amount of rupture life that has been expended, a total of 6% of the 1% creep rupture life of the disk has been used.

Conclusions & Recommendations

Examination of the disk microstructure taken from replicas reveal a consistent grain size between the disk roots and the body of the disk on both the inlet and exhaust faces. No evidence of creep damage or exposure to temperatures beyond the service temperature could be found. The hardness at all locations was also consistent which provides further proof that the disk was not exposed to excessive temperatures.

Two blades were taken from the unit for further examination and destructive testing, and one of these blades was re-solution treated and aged before testing. A comparison of the microstructures between the blades shows a less discrete grain boundary of the service condition blade as well as possible evidence of precipitates forming at the grain boundaries. The re-heat treated blade had a longer time to rupture than the service condition blade during stress rupture testing, however, both blades meet the stress rupture requirements of Elliott MS-487A and both samples fractured in the smooth location.

Stress Relaxation Testing (SRT) showed that there has been a slight reduction in the creep strength in the service

condition blade in comparison to the re-heat treated blade. The creep strength of the service condition blade still compares well to standard Waspaloy SRT samples tested under the same conditions at the service temperature of the unit. Constant Displacement Rate (CDR) testing reveals that the service condition blade does display a reduction in notch ductility in comparison to the re-heat treated blade, however the stress rupture test indicated that the material was not severely notch sensitive due to the failure occurring in the smooth section of the specimen.

Stress rupture testing in the presence of catalyst provided showed that the Waspaloy was not subject to corrosive attack by any impurities in the catalyst during the test.

Cross-sectional samples taken from the inside radius of the top blade root of the service condition blade revealed that a sulfide corrosion wedge had formed. This corrosion wedge had a depth of 0.0043 inches, and fracture mechanics performed on the blade root show that this corrosion wedge will not reach a critical depth of 0.150 inches during the life of unit if conditions remain constant.

The conclusion from the remaining life assessment testing is that the disk is suitable for future service under the current operation conditions of the unit. The current condition of the disk does not indicate a significant reduction in the creep strength of the material or any significant changes to the microstructure.

REFERENCES

Baik, J.M., Kameda, J., and Buck, O., 1983, *Scripta Met.*, Vol 17, p. 1143-1147.

Birks, N. and Meier, G.H., 1983, Introduction to High Temperature Oxidation of Metals, Edward Arnold.

Biss, V.A. and Wada, T., 1985, "Microstructural Changes in 1Cr-0.5Mo Steel after 20 Years of Service," Metallurgical Transactions A, Vol. 16A, January, pp. 100-115.

Bruscato, R.M., 1970, Welding J, Vol. 35, page 148S.

Bush, S.H., 1982, "Failures in Large Steam Turbine Rotors, in Rotor Forgings for Turbines and Generators," R.I. Jaffe, Ed., Pergamon Press, New York, p. I-1 to I-27.

Carlton, R.G., Gooch, D.J., and Hawkes, B.M., 1967, The Central Electrical Generating Board Approach to "The Determination of Remanent Life of High Temperature Turbine Rotors," I. Mech E. paper C300/87.

Demirkol, M., 1999, "On the Creep Strength-Rupture Ductility Behavior of 1.25Cr-0.5Mo Low Alloy Steel," Tr. J. of Engineering and Environmental Science, 23, pp. 389-401.

Dowson, P., 1994, "Fitness for Service of Rotating Turbomachinery Equipment," 10th Annual North American Welding Research Conference, Columbus, Ohio, October 3-5.

Dowson, P., 1995, "Fracture Mechanics Methodology Applied to Rotating Components of Steam Turbines and Centrifugal Compressors," Third International Charles Parson Turbine Conference, Materials Engineering in Turbine and Compressors, Vol. 2, pp. 363-375.

Dowson, P. and Rishel, D., 1995, "Factor and Preventive Measures Relative to the High Temperature Corrosion of Blade/Disk Components in FCC Power Recovery Turbines," Proceedings of the 24th Turbomachinery Symposium, September, pp. 11-26.

Dowson, P. and Stinner, C., 2000, "The Relationship of Stress and Temperature on High-Temperature Corrosion Fracture Mechanics of Waspaloy in Various Catalyst Environments," Proceedings of High Temperature Corrosion and Protection, Materials at High Temperatures 18(2), pp. 107-118.

Foulds, J.R., Jewett, C.W., and Viswanathan, R., 1991, "Miniature Specimen Test Technique for FATT," ASME/1EEE Joint Power Generator Conference, Paper No. 91 – JPGC – PWR-38, ASME, New York.

Goldhoff, R.M. and Woodford, D.A., 1972, "The Evaluation of Creep Damage in CrMoV Steel in Testing for Prediction of Material Performance in Structure and Components," STP 515 American Society for Testing and Materials, Philadelphia, p. 89-106.

Kadoya, Y., et al., 1991, "Nondestructive Evaluation of Temper Embrittlement in CrMoV Steel," ASME/JEEE Joint Power Generator Conference, Paper PWR-Vol. 13, ASME, New York.

Neubauer, E. and Wadel, V., 1983, "Rest Life Estimation of Creep Components by Means of Replicas", Advances in Life Prediction Methods, Ed., Woodford, D.A., and Whitehead, J.E., (New York: ASME), pp. 307-314.

Newhouse D.L., et al., 1972, in "Temper Embrittlement of Alloy Steels" ASTM STP 499, pp. 3-36.

Pope, J.J. and Genyen, D.D., 1989, International Conference on Fossil Power Plant Rehabilitation, ASM International, pp. 39-45.

Saxena A., 1998, Nonlinear Fracture Mechanics for Engineers, p. 449.

Schwant R.C. and Timo, D. P., 1985, "Life Assessment of General Electric Large Steam Turbine Rotors in Life Assessment and Improvement of Turbogenerator Rotors for Fossil Plants," Viswanathan, R., Ed., Pergamon Press, New York, p. 3.25 – 3.40.

Viswanathan, R. and Gehl, S.M., 1991, "A Method for Estimation of the Fracture Toughness of CrMoV Rotor Steels Based on Composition," ASME Transaction, Journal of Engineering Mat. and Tech., Vol. 113, April, pp. 263.

Viswanathan, R. and Gehl, S.M., 1992, "Life-Assessment Technology for Power Plant Components," JOM, February, pp. 34-42.

Viswanathan, R. and Jaffee, R.J., 1983, "Toughness of Cr-Mo-V Steels for Steam Turbine Rotors," ASME. Journal of Engineering Mat. and Tech., Vol. 105, October, p. 286-294.

Viswanthan R. and Wells, C. H., 1995, "Life Prediction of Turbine Generator Rotors," Third International Charles Parsons Turbine Conference, Materials Engineering in Turbines and Compressors, Vol. 1, pp. 229-264.

Watanabe, J. and Murakami, Y., 1981, "Prevention of Temper Embrittlement of CrMo Steel Vessels by the Use of Low Si Forged Steels," American Petroleum Institute, Chicago, IL, p. 216.

Woodford, D.A., 1993, Materials and Design, Vol. No. 4, p. 231.

Woodford, D.A., Von Steele, D.R., Amberge, K., and Stiles, D., 1992, "Creep Strength Evaluation for IN738 Based on Stress Relaxation" from Superalloys, The Minerals, Metals and Material Society, Ed., Antolovich, S.D., Stusned, R.W., Mackay, R.A., Anton, D.L., Khan, T., Kissinger, R.D., Klarstrom, D.L., pp. 657-663.